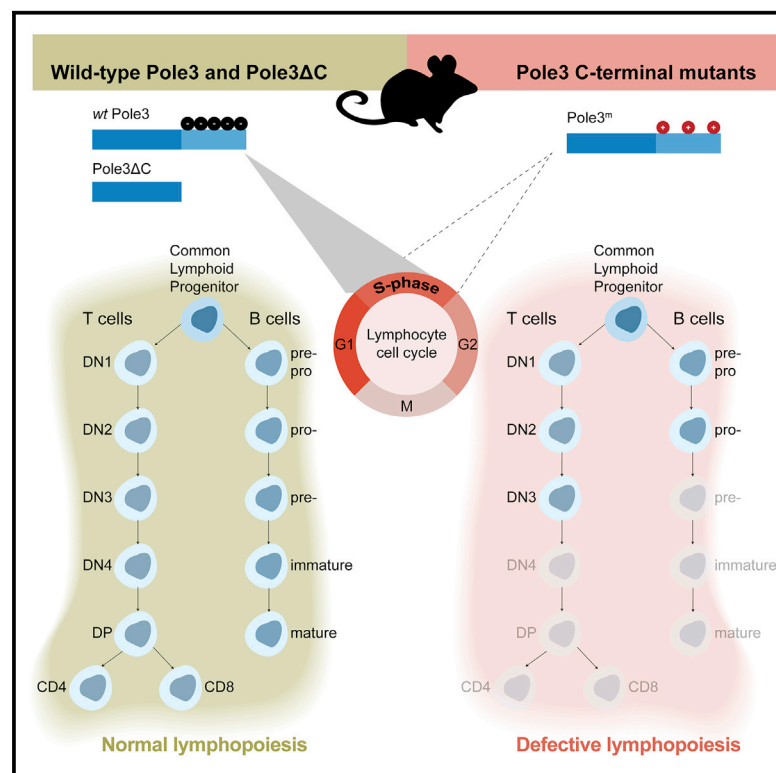


# Lymphocyte-Specific Function of the DNA Polymerase Epsilon Subunit Pole3 Revealed by Neomorphic Alleles

## Graphical Abstract



## Authors

Iliana Siamishi, Norimasa Iwanami, Thomas Clapes, Eirini Trompouki, Connor P. O'Meara, Thomas Boehm

## Correspondence

boehm@ie-freiburg.mpg.de

## In Brief

Siamishi et al. reveal a non-replicative function of Pole3 during mouse *in vivo* lymphopoiesis. Pole3 C-terminal mutants exhibit perturbations at specific stages of T and B cell development. Cell cycle defects expose a function of Pole3 in the regulation of S-phase progression in lymphocytes.

## Highlights

- Pole3 has a non-replicative function during mouse lymphopoiesis
- The acidic C terminus of Pole3 regulates the function of the N-terminal domain
- Pole3 C-terminal mutants exhibit stage-specific blocks of T and B cell development
- Pole3 mutant thymocytes progress faster through the S-phase of the cell cycle



## Article

# Lymphocyte-Specific Function of the DNA Polymerase Epsilon Subunit Pole3 Revealed by Neomorphic Alleles

Ilana Siamishi,<sup>1,2</sup> Norimasa Iwanami,<sup>1,4</sup> Thomas Clapes,<sup>3</sup> Eirini Trompouki,<sup>3</sup> Connor P. O'Meara,<sup>1</sup> and Thomas Boehm<sup>1,5,\*</sup>

<sup>1</sup>Department of Developmental Immunology, Max Planck Institute of Immunobiology and Epigenetics, 79108 Freiburg, Germany

<sup>2</sup>Faculty of Biology, University of Freiburg, 79108 Freiburg, Germany

<sup>3</sup>Department of Cellular and Molecular Immunology, Max Planck Institute of Immunobiology and Epigenetics, 79108 Freiburg, Germany

<sup>4</sup>Present address: Center for Bioscience Research and Education, Utsunomiya University, Utsunomiya, Tochigi 321-8505, Japan

<sup>5</sup>Lead Contact

\*Correspondence: boehm@ie-freiburg.mpg.de

<https://doi.org/10.1016/j.celrep.2020.107756>

## SUMMARY

Immunodeficiencies are typically caused by loss-of-function mutations in lymphocyte-specific genes. Occasionally, mutations in ubiquitous general-purpose factors, including those affecting essential components of the DNA polymerase epsilon (POLE) holoenzyme, have cell-type-specific consequences. POLE3, one of the four components of the POLE holoenzyme, features a histone fold domain and a unique acidic C terminus, making it a particularly attractive candidate mediating cell type-specific activities of POLE. Mice lacking Pole3 survive up to late embryonic stages, indicating that this subunit is dispensable for DNA replication. The phenotypes of viable hypomorphic and neomorphic alleles are surprisingly tissue restricted and reveal a stage-specific function of the histone fold domain of Pole3 during T and B cell development. Gradual introduction of positively charged residues into the acidic C terminus leads to peripheral lymphopenia of increasing severity. Our findings serve as a paradigm to understand the molecular basis of cell-type-specific non-replicative functions of the ubiquitous POLE complex.

## INTRODUCTION

Cell differentiation in the developing organism is orchestrated by a complex interplay of extrinsic and cell-intrinsic factors. Lymphocytes of the T and B cell lineages fall into a special category, as they are the only known cell types for which programmed DNA rearrangements constitute an essential aspect of their maturation process. Therefore, the list of recessive genetic defects that impair lymphocyte function contains not only genes encoding molecules involved in their communication with the environment, such as the IL7 receptor (Puel et al., 1998), but also genes encoding key factors of DNA recombination and repair processes, such as the recombination activating genes RAG1 and RAG2 (Mombaerts et al., 1992; Schwarz et al., 1996), DNA cross-link repair protein 1c (DCLRE1C; also known as ARTEMIS) (Moshous et al., 2001), ligase IV (LIG4) (Grawunder et al., 1998; O'Driscoll et al., 2001), the catalytic subunit of the DNA-dependent kinase (PRKDC) (van der Burg et al., 2009; Woodbine et al., 2013), and others.

In recent studies, immunodeficiency was found to be associated with mutations in genes encoding general-purpose factors, such as those required for DNA replication. For instance, mutations in the gene encoding the catalytic subunit of DNA polymerase epsilon (POLE), *POLE1*, are associated with multi-organ pathology, including immunodeficiency (FILS syndrome and

IMAGe syndrome with variable immunodeficiency) (Logan et al., 2018; Pachlopnik Schmid et al., 2012). A mutation in the gene encoding the POLE2 subunit of POLE also causes combined immunodeficiency (Frugoni et al., 2016). These findings suggest the possibility that specific mutations in other components of the POLE holoenzyme complex might also result in lymphocyte-lineage defects and may even serve as the molecular link between ubiquitous and cell type-specific functions.

POLE is an evolutionarily conserved, four-component holoenzyme that synthesizes the leading strand during DNA replication (Kunkel and Burgers, 2008). POLE1 is the catalytic subunit of the holoenzyme, with the POLE2 subunit representing the second essential component (Araki et al., 1991a; Jaszczur et al., 2008). The two accessory subunits of the complex, POLE3 and POLE4, form a heterodimer through their histone fold domains (Li et al., 2000). They were shown to contribute to the stability of the POLE holoenzyme, but at least in unicellular organisms, they are not absolutely essential for growth, as depletion of the yeast *Pole3* and *Pole4* homologs does not compromise DNA replication (Araki et al., 1991b; Ohya et al., 2000). It has been suggested that POLE3 and POLE4 may serve functions other than participating in DNA replication; this notion is supported by the observation that POLE3 (also known as p17) co-purifies with proteins of the chromatin remodeling complex ACF1-ISWI (Kukimoto et al., 2004; Poot et al., 2000). The POLE3 subunit



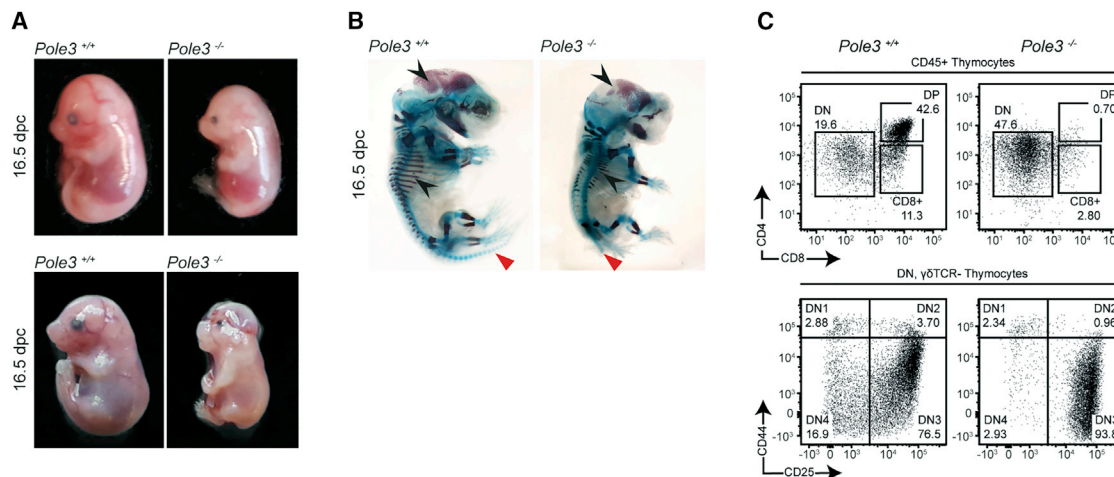


**Figure 1. Late Embryonic Lethality of *Pole3* Deficiency**

(A) Gross appearance of *Pole3*<sup>+/+</sup> and *Pole3*<sup>-/-</sup> littermate embryos from two independent experiments at 16.5 days post-coitum (DPC) (top and bottom panels), illustrating the small size and cranial defects (bottom, indicated by white arrowhead) of *Pole3*<sup>-/-</sup> embryos.

(B) Alcian blue-alizarin red staining of *Pole3*<sup>+/+</sup> and *Pole3*<sup>-/-</sup> littermate embryos at 16.5 DPC. Note the incomplete cranial ossifications and shorter rib bones in the *Pole3*<sup>-/-</sup> embryo (alizarin red, indicated by black arrowheads); fusion of vertebrae and the shorter tails of the *Pole3*<sup>-/-</sup> embryo are also evident (Alcian blue, indicated by red arrowheads).

(C) Flow cytometric profiles of thymocytes of *Pole3*<sup>+/+</sup> and *Pole3*<sup>-/-</sup> embryos at 16.5 DPC. The distribution of CD8<sup>+</sup> SP, CD4<sup>+</sup>CD8<sup>+</sup> (DP), and CD4<sup>-</sup>CD8<sup>-</sup> (DN) thymocytes indicates an accumulation of DN and the loss of DP and intermediate SP (ISP) cells in the mutant (upper panels); the distribution of the DN ( $\gamma\delta$ TCR<sup>+</sup>) thymocyte populations characterized by CD44 and CD25 indicate an accumulation of DN3 cells. The percentages of cells in each gate are indicated.

differs from the POLE4 subunit by the presence of a C-terminal domain that is enriched for negatively charged amino acids. This feature can be found in all vertebrate orthologs; however, its function is unknown. We hypothesized that this protein domain of POLE3 may link the general replicative functions of the POLE holoenzyme to cell type-specific activities.

Here, we describe our experiments aimed at elucidating the enigmatic functions of POLE3. We found that mice homozygous for a null allele of *Pole3* exhibit embryonic lethality only in the last stages of gestation, clearly demonstrating that this protein is not essential for cell division; interestingly, this phenotype is reminiscent of that of *Pole4*-deficient mice (Bellelli et al., 2018b). The phenotypes of an allelic series of *Pole3* reported herein demonstrate that the acidic tail of the POLE3 protein is indeed involved in mediating cell type-specific functions. Conversion of the negative charge of the C-terminal domain into a net positive charge results in a cell-autonomous, stage-specific block of T and B lymphocyte differentiation in the thymus and bone marrow, respectively, leading to severe peripheral lymphopenia. Collectively, our work suggests a possible mechanism through which the DNA POLE holoenzyme regulates the differentiation of lymphoid cells.

## RESULTS

### Late Embryonic Lethality of *Pole3* Deficiency

We took a genetic approach to investigate the physiological role of POLE3 in the mouse. As a first step, we examined the consequences of inactivating the *Pole3* gene in the germline of C57BL/6 mice. Mice homozygous for the *Pole3*<sup>tm1(KOMP)Vlcg</sup> null allele (Figure S1A) died during late stages of embryogenesis around

embryonic day (E) 16.5. *Pole3*-deficient embryos were smaller in size than their wild-type littermates and sometimes exhibited severe cranial defects (Figure 1A). It is possible that the late embryonic lethality in mice with *Pole3* and *Pole4* (Bellelli et al., 2018b) deficiencies is the result of partial functional redundancies between these two accessory subunits of the POLE holoenzyme, as they both share a characteristic histone fold domain (Figure S1B). Analysis of the skeletal structures of mutant embryos revealed delayed ossification of the rib and cranial bones; the vertebrae are fused, resulting in shorter tails (Figure 1B). Of note, mice heterozygous for the mutant allele were essentially normal (data not shown). Taken together, the complete loss of *Pole3* gene function leads to severe defects during embryonic development, which eventually compromise the viability of mutant mice. Importantly, however, our results indicate that *Pole3* is not absolutely essential for the DNA replication function of the POLE holoenzyme.

Given the association of skeletal defects and immunodeficiency observed in human patients harboring a hypomorphic mutation in the gene encoding the catalytic subunit of the POLE holoenzyme, *POLE1* (Pachlopnik Schmid et al., 2012), we examined *Pole3*-deficient mice for the presence of defects in the lymphoid compartment. At E16.5, the thymi of *Pole3*<sup>-/-</sup> embryos were essentially devoid of double-positive CD4<sup>+</sup>CD8<sup>+</sup> (DP) thymocytes; the majority of cells had the cell surface phenotype of DN3 (CD44<sup>-</sup>CD25<sup>+</sup>) precursors (Figure 1C); heterozygous mice were indistinguishable from wild-type siblings (data not shown). These results are compatible with a block in transition from the DN3 to the DN4 (CD44<sup>-</sup>CD25<sup>-</sup>) stage during T cell differentiation in the thymus or, alternatively, with a general developmental delay of mutant animals. These results reinforce

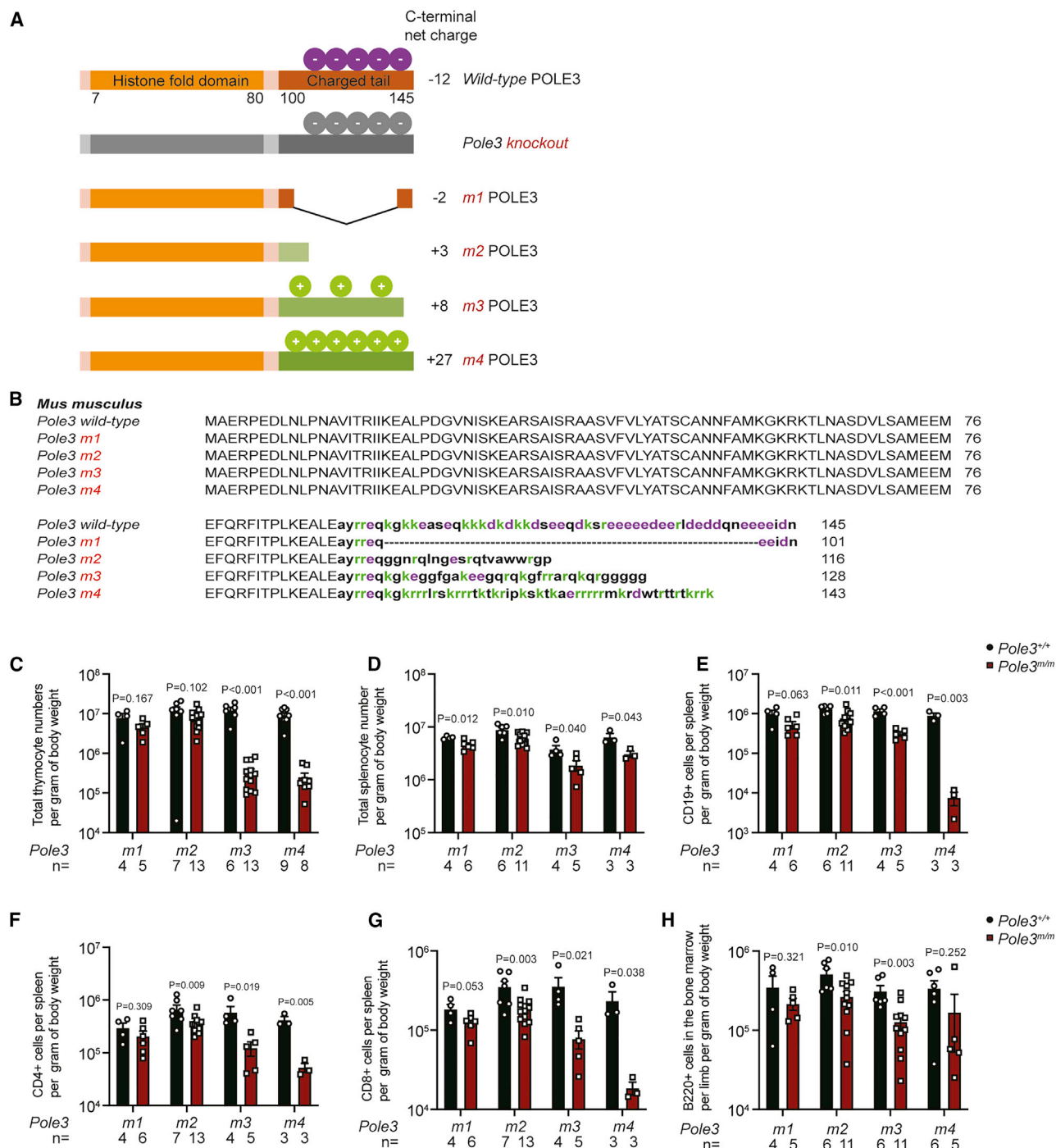


**Figure 2. Functional Role of the Pole3 C Terminus**

(A) Schematic representations of the wild-type Pole3 protein and its variants studied here; the estimated values of the net charge of the C-terminal domains are indicated.

(B) Alignment of predicted protein sequences of the *Pole3* allelic variants. The sequence of the C-terminal domain is highlighted by lowercase characters. Negatively charged residues are shown in purple and positively charged residues in green fonts.

(C) Total thymocyte numbers per gram of body weight in *Pole3* allelic variants at 4–8 weeks of age. Results from male and female mice are pooled, as there was no difference between sexes; each data point represents one mouse.

(D) Total splenocyte numbers per gram of body weight in *Pole3* allelic variants at 4–8 weeks of age.

(E–G) Absolute numbers of CD19<sup>+</sup> B cells (E), CD4<sup>+</sup> T cells (F), and CD8<sup>+</sup> T cells (G) per gram of body weight in the spleen of 4- to 8-week-old *Pole3* mice.

(legend continued on next page)



the notion of a multi-organ pathology in *Pole3*-deficient embryos but also demonstrate that tissues differ remarkably in their sensitivity to loss of *Pole3*. Interestingly, lymphocyte defects in mice were recently also described after inactivation of the gene encoding the fourth component of POLE, namely, *Pole4*; the lymphocyte phenotype was part of a complex syndrome dominated by a severe growth defect and interpreted to be the result of higher sensitivity of specific cell types to compromised stability of the POLE holoenzyme (Bellelli et al., 2018b). Because the phenotype observed in *Pole3* null mice described here is very similar to that described for *Pole4* null mice, we propose that the pathology in these mutant mice is the result of (at least partially) overlapping molecular perturbations. As mice lacking functional *Pole3* or *Pole4* genes survive into late gestation, they may substitute for each other for certain aspects of their non-replicative activities.

### Functional Role of the *Pole3* C Terminus

Although the precise sequences differ, all vertebrate POLE3 proteins possess an acidic C-terminal, which is encoded in exon 4 (Figure S1C). It distinguishes them from vertebrate POLE4 proteins, which lack this type of C-terminal extension (Figure S1B). This structural difference led us to hypothesize that the C terminus of *Pole3* has a distinct function, possibly unrelated to the DNA replication process. To explore this possibility, we first created a *Pole3* variant (henceforth designated *Pole3*<sup>m1</sup>) with an internal deletion encompassing most of exon 4 (Figure S1D; Figures 2A and 2B). As a result, the predicted protein of the mutant allele lacks 45 amino acids (aa), removing residues 97–140 of this 145 aa protein encoding the two C-terminal  $\alpha$  helices (Figure 2B). Mice homozygous for this allele are viable, are born at the expected Mendelian ratios (Table S1), and exhibit neither obvious developmental defects nor postnatal growth delay (Table S2). With respect to lymphoid development, we observed a small but non-significant reduction in the number of thymocytes (Figure 2C), peripheral lymphocytes in the spleen (Figures 2D–2G), and B220<sup>+</sup> B cells in the bone marrow (Figure 2H); the cell numbers in *Pole3*<sup>+/m1</sup> heterozygous mutant mice did not differ from wild-types.

In cultured cells, the C-terminal tail of *Pole3* is required for replication-dependent nucleosome remodeling through the interaction with the histones H3 and H4 (Bellelli et al., 2018a). The detrimental effect of the tailless *Pole3* version in this setting contrasts with the mild effect of a similar protein mutant *in vivo*, suggesting the presence of efficient compensatory mechanism(s) operating during normal development but unattainable in the *in vitro* situation. To circumvent this potential complication in the phenotypic analysis of *Pole3* variants in the organismal context, we probed the function of the acidic tail of *Pole3* more directly. Specifically, we chose to change the amino acid composition of the C terminus with the aim of generating neomorphic versions of *Pole3*, in the hope that they would be insensitive to the presumptive *in vivo* compensation mechanism(s). To

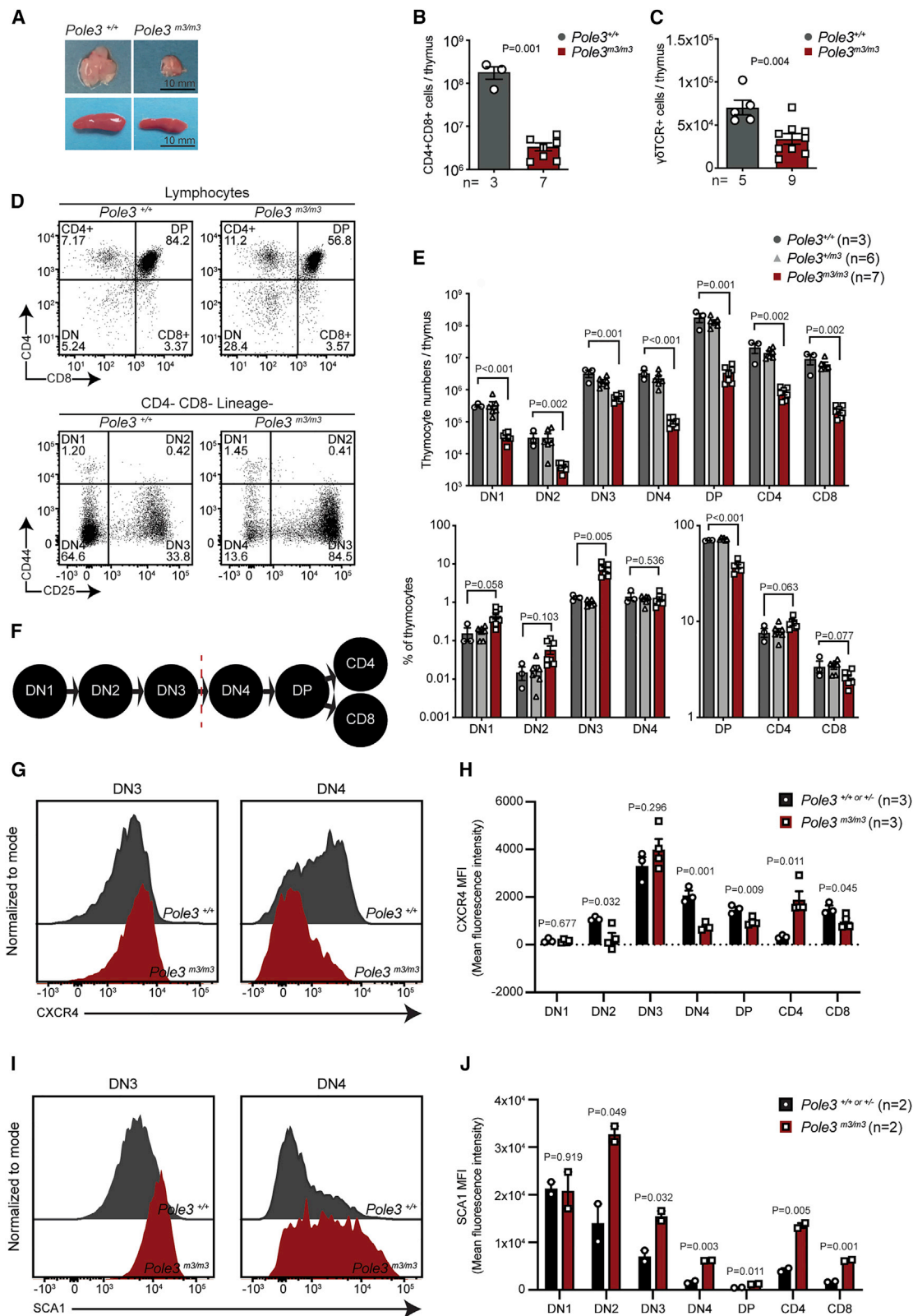
this end, we generated a series of mutations in exon 4 of the *Pole3* gene using the CRISPR-Cas9 technology, three of which are discussed here. An initial replacement modification (this allele is henceforth referred to as *Pole3*<sup>m2</sup>) retains amino acid residues 1–95 of the wild-type protein, but then appends 20 aa residues of unrelated sequence (Figures 2A and 2B). With respect to the overall charge of the C terminus (the relevant part of the protein considered for this calculation is indicated in lowercase letters in Figure 2B), the m2 modification introduces a net charge of +3 compared with the net charge of –12 for this domain in the wild-type protein; in this respect, it is similar to the internal deletion mutant, which has a net charge of –2 (Figure 2A). Mice homozygous for the *Pole3*<sup>m2</sup> allele were born at the expected frequency (Table S1), with no gross developmental defects, and were viable. However, with respect to lymphoid development, a comparison of *Pole3*<sup>m1</sup> and *Pole3*<sup>m2</sup> alleles in the state of homozygosity revealed a more pronounced impairment of lymphocyte development in the latter, although the magnitude of the reduction was still only moderate (Figures 2C–2H). Collectively, the results obtained with *Pole3*<sup>m1</sup> and *Pole3*<sup>m2</sup> alleles indicate that the variant C terminus of unrelated sequence as found in the *Pole3*<sup>m2</sup> alleles may be subject to the same compensation process as the *Pole3*<sup>m1</sup> allele.

Therefore, in order to generate more effective neomorphic alleles, we focused on mutant proteins with greater net positive charge of the C terminus. We examined two additional mutant variants that resulted in net charges of +8 (*Pole3*<sup>m3</sup>) and +27 (*Pole3*<sup>m4</sup>), respectively (Figures 2A and 2B). In contrast to the situation of *Pole3*<sup>m1</sup>, *Pole3*<sup>m2</sup>, and *Pole3*<sup>m3</sup> alleles, we found that the homozygous constellation of *Pole3*<sup>m4</sup> was associated with severely compromised viability. At the age of 3 weeks, only about 10% of the expected number of *Pole3*<sup>m4/m4</sup> mice were observed; by contrast, the *Pole3*<sup>+/+</sup> and *Pole3*<sup>+/m4</sup> genotypes were found in a 1:2 ratio, indicating that the *Pole3*<sup>m4</sup> allele is not dominant over the wild-type allele (Table S1). The loss of *Pole3*<sup>m4/m4</sup> homozygotes occurs during embryogenesis and/or perinatally, although the precise time point of mutant death was not determined. The mechanism(s) underlying this impaired survival are unclear; the distinct genetic backgrounds afforded by FVB and C57BL/6 mice had no effect on the survival rate.

Of note, surviving *Pole3*<sup>m3/m3</sup> and *Pole3*<sup>m4/m4</sup> homozygous mutants lacked gross morphological abnormalities, except minor skeletal deformities in the *Pole3*<sup>m4/m4</sup> mutant mice that were apparent on the FVB background (Figures S2A and S2B). With respect to the lymphoid system, mice homozygous for *Pole3*<sup>m3</sup> and *Pole3*<sup>m4</sup> alleles exhibited drastic reductions in the numbers of thymocytes, peripheral lymphocytes, and B220<sup>+</sup> B cells in the bone marrow (Figures 2C–2H); in these respects, mice heterozygous for the *Pole3*<sup>m3</sup> and *Pole3*<sup>m4</sup> alleles were found to be indistinguishable from wild-type littermates (data not shown). Because *Pole3*<sup>m3/m3</sup> homozygotes occupy an intermediate position in the phenotypic spectrum of *Pole3* C-terminal mutants, we focused subsequent studies on the *Pole3*<sup>m3</sup> allele.

(H) Total number of B220<sup>+</sup> cells in the bone marrow of adult *Pole3* mice isolated from one lower limb (cells from tibia, femur, and pelvis combined) and given as per gram of body weight.

In (C)–(H), the allele tested is shown underneath the bars with mean  $\pm$  SEM indicated; wild-type and homozygous mutant animals are compared (p values of t tests are indicated); each data point represents one mouse.



(legend on next page)

The expression levels of the mutant Pole3 proteins could not be determined, because all available anti-Pole3 antisera fail to specifically react with the N terminus (data not shown); however, transcripts emanating from the mutant alleles are readily detectable (Figure S2C).

### Stage-Specific Defects of T and B Cell Differentiation in Pole3 C-Terminal Mutant Mice

*Pole3*<sup>m3/m3</sup> mice exhibited smaller thymi and spleens than their wild-type littermates (Figure 3A). To avoid the confounding effects of thymic involution, all mice were age matched and used at 4–12 weeks of age; the *Pole3* mutant phenotypes were still detectable in aged mice (data not shown). We found that hematopoietic precursor subsets (HSCs, MPP1, MPP2, MPP3, MPP4, and CLP) are not affected in *Pole3*<sup>m3/m3</sup> mutants (Figures S2D–S2G), indicating that the development of T and B cells is affected at later stages of lymphoid development. The intrathymic T cell development of *Pole3*<sup>m3/m3</sup> is distinguished by a 50-fold reduction in the absolute numbers of DP T cells (Figure 3B); in contrast, the reduction of  $\gamma\delta$  T cells is only about 2-fold (Figure 3C), pointing to differences in the sensitivity of  $\alpha\beta$  and  $\gamma\delta$  T cell lineages to the mutant Pole3 proteins. In the mutants, the proportion of DP thymocytes is decreased, whereas the proportion of double-negative (DN) precursors is increased (Figure 3D); the accumulation of cells at the DN3 T cell stage suggests a failure to efficiently proceed to the DN4 stage (Figures 3D–3F). The aberrations in intrathymic T cell differentiation are magnified in *Pole3*<sup>m4/m4</sup> homozygous mice (Figure S3). In both *Pole3*<sup>m3/m3</sup> and *Pole3*<sup>m4/m4</sup> mice, high levels of apoptosis were found in DN1, DN2, and DN3 thymocytes (an effect more pronounced in the *Pole3*<sup>m4/m4</sup> mutants) (Figure S4), likely contributing to the reduced cell numbers in these subsets. However, from the DN4 stage onward, the differences in viability between wild-type and mutant cells are less pronounced, suggesting that the sensitivity to Pole3 mutations changes over developmental time.

The levels of Cxcr4 expression in *Pole3*<sup>m3/m3</sup> mutant thymocytes are lower than those of their wild-type counterparts (Figures 3G and 3H). Of note, we observed a rapid loss of Cxcr4 expression from the DN3 to the DN4 stage (Figures 3G and 3H), during which Cxcr4 signals physiologically combine with signals emanating from the pre-TCR to promote survival and differentiation beyond the  $\beta$ -selection checkpoint (Tramont et al.,

2010). However, several lines of evidence suggest that the differentiation trajectory of thymocytes as such is not impaired. The levels of intracellular TCR- $\beta$  chains in DN3 cells (Figure S5A) and the density of TCR- $\beta$  at the cell surface of DP and single-positive (SP) thymocytes (Figures S5B and S5C) of mutant mice are indistinguishable from wild-type littermates. These findings and evidence for rearrangement at the *Tcrb* locus (Figure S5D) suggest that failure of VDJ recombination per se does not underlie the T cell differentiation defect in the mutant mice, although we cannot exclude subtle alterations in the rearrangement process. Moreover, expression of an  $\alpha\beta$  TCR transgene (Oxenius et al., 1998) failed to rescue the T cell-deficient phenotype of Pole3 mutant mice (Figure S5E).

In the bone marrow of *Pole3*<sup>m3/m3</sup> mice, hematopoietic precursor subsets exhibited increased expression levels of the hematopoietic marker stem cell antigen (Sca1; also known as Ly6A/E) (Figure S5F), which appears to persist into later stages of lymphoid differentiation (Figures 3I and 3J). This phenotype is functionally relevant, as loss of Sca1 expression is critical for the transition through the DN thymocyte stages (Bamezai et al., 1995; Henderson and Bamezai, 2003). Collectively, low Cxcr4 and high Sca1 levels might synergize to impair the efficiency of T cell development in *Pole3*<sup>m3/m3</sup> mice.

Analysis of B cell development in the bone marrow of *Pole3*<sup>m3/m3</sup> mice indicated an almost 3-fold reduction of pre-B cell numbers (B220<sup>+</sup>IgM<sup>−</sup>CD43<sup>−</sup>) (Figures 4A and 4B); accordingly, the numbers of IgM<sup>+</sup> immature and re-circulating B lymphocytes were also reduced (Figures 4A and 4B). These data suggest an incomplete block in the transition from the pro-B (B220<sup>+</sup>IgM<sup>−</sup>CD43<sup>+</sup>CD24<sup>+</sup>) to the pre-B cell stage (Figure 4C), functionally analogous to the impaired DN3/DN4 transition in thymocytes. Mice homozygous for the *Pole3*<sup>m4/m4</sup> allele exhibited similar, albeit more pronounced defects of B cell development in the bone marrow (Figures S6A and S6B). We found that pre-B and immature B cells (but not pre-pro-, pro-, or re-circulating B cells in the bone marrow) exhibit significant reduced viabilities in *Pole3*<sup>m3/m3</sup> (an effect that is even more pronounced in *Pole3*<sup>m4/m4</sup>) mice (Figure S4), reminiscent of the equivalent situation in thymocytes. However, under the conditions of our conventional mouse house, mature peripheral B cells in *Pole3*<sup>m3/m3</sup> differentiate into switched memory and germinal center B cells (Figures S6C–S6E); accordingly, germinal centers are readily detectable in the spleen (Figure S6F), and serum

### Figure 3. Stage-Specific Defects of T Cell Differentiation in Pole3 C-Terminal Mutant Mice

(A) Representative images of thymus (top) and spleen (bottom) of adult mice (7 weeks of age).  
(B) Total numbers of CD4<sup>+</sup>CD8<sup>+</sup> (DP) cells in adult thymi.  
(C) Total numbers of  $\gamma\delta$  TCR<sup>+</sup> T cells in adult thymi.  
(D) Flow cytometric analysis of the distribution of thymocyte populations in adult mice stained with antibodies against CD4<sup>+</sup> and CD8<sup>+</sup> (top panels); for the analysis of DN progenitor thymocytes (bottom panels), they were gated on CD4<sup>−</sup>CD8<sup>−</sup>Lineage marker<sup>−</sup> (B220<sup>−</sup>CD11b<sup>−</sup>CD11c<sup>−</sup>NK1.1<sup>−</sup> $\gamma\delta$ TCR<sup>−</sup>) cells. The percentages of cells in each gate are shown.  
(E) Total numbers (top panel) and frequencies (bottom panel) of thymocyte populations in adult mice of the indicated genotypes.  
(F) Cartoon illustrating the developmental stages of T cell differentiation in the thymus; the dotted line marks the differentiation block observed in *Pole3*<sup>m3/m3</sup> mice.  
(G) Representative histograms of surface expression of CXCR4 in DN3 and DN4 thymocytes.  
(H) Calculation of mean fluorescence intensity (MFI) of CXCR4 cell surface signal on intrathymic T cells.  
(I) Representative histograms of surface expression of SCA1 in DN3 and DN4 thymocytes.  
(J) Calculation of mean fluorescence intensity (MFI) of SCA1 cell surface signal on intrathymic T cells.  
In (B)–(J), mean  $\pm$  SEM is indicated; wild-type and homozygous mutant animals are compared; in (G)–(J) heterozygous animals are also used as controls (p values of t tests are indicated); each data point represents one mouse.

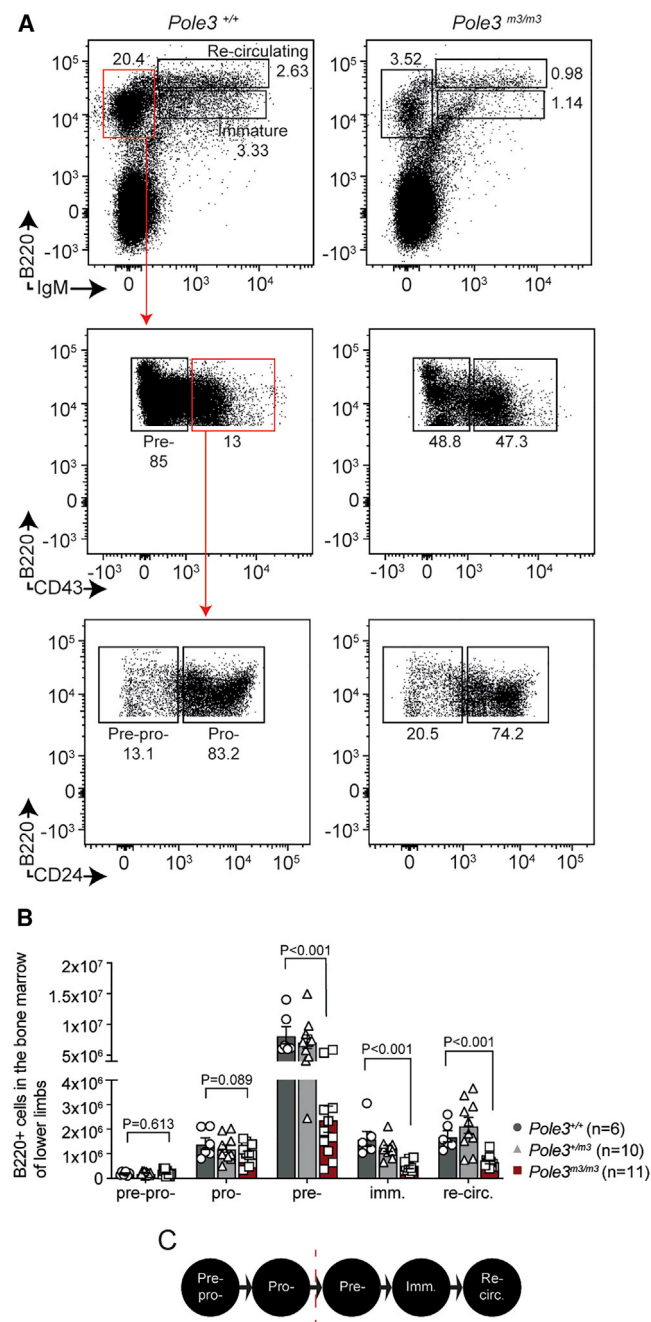


**Figure 4. Stage-Specific Defects of B Cell Differentiation in *Pole3* C-Terminal Mutant Mice**

(A) Gating strategy for flow cytometric analysis of B cell development in the bone marrow of *Pole3*<sup>+/+</sup> and *Pole3*<sup>m3/m3</sup> mice. Cells are classified as re-circulating B cells (B220<sup>high</sup>IgM<sup>+</sup>), immature B cells (B220<sup>high</sup>IgM<sup>+</sup>), pre-B cells (B220<sup>high</sup>IgM<sup>+</sup>CD43<sup>+</sup>), pre-pro-B cells (B220<sup>high</sup>IgM<sup>+</sup>CD43<sup>+</sup>CD24<sup>+</sup>), and pro-B cells (B220<sup>high</sup>IgM<sup>+</sup>CD43<sup>+</sup>CD24<sup>+</sup>). Numbers indicate percentages of cells in each gate.

(B) Total numbers of B220<sup>+</sup> cells in each B cell stage. The numbers are representative of whole bone marrow from the lower limbs (cells from femur, tibia, and pelvis combined) of adult mice. Bars denote mean  $\pm$  SEM; wild-type and homozygous mutant animals are compared (p values of t tests are indicated); each data point represents one mouse.

immunoglobulin levels in *Pole3*<sup>m3/m3</sup> are comparable with wild-type levels (Figure S6G).

Collectively, the detrimental lymphocyte-specific outcomes of *Pole3*<sup>m3</sup> and *Pole3*<sup>m4</sup> alleles suggest that mutant POLE3 proteins carrying a positively charged C terminus have neomorphic properties, subverting the compensatory mechanism alleviating the effects of *Pole3*<sup>m1</sup> and *Pole3*<sup>m2</sup> alleles. Although the efficiency of B cell development is drastically reduced, mature B cells in the mutants do not appear to be functionally impaired.

### Pole3 Acts in a Cell-Autonomous and Cell Type-Specific Manner during Lymphocyte Development

To examine the cell autonomy of the T and B cell phenotype in *Pole3*<sup>m3/m3</sup> mice, competitive whole bone marrow transplantations of allotype-tagged wild-type and mutant cells were conducted (Figure 5A). To achieve equivalence of biological potency, the mixtures were constructed such that they contained the same number of hematopoietic stem cells (HSCs) (Lineage marker<sup>neg</sup>Sca1<sup>high</sup>c-Kit<sup>high</sup>CD150<sup>+</sup>CD34<sup>+</sup>CD48<sup>+</sup>Fli2<sup>+</sup>) in both donor sources. The analysis of peripheral blood samples of recipient mice in 4 week intervals revealed that the overall hematopoietic capacity of *Pole3*<sup>m3/m3</sup> bone marrow progenitors appeared to be inferior to that of their wild-type counterparts (Figure 5B).

This effect is not the result of an impaired homing capacity of *Pole3*<sup>m3/m3</sup> HSCs to the bone marrow, as the number of transferred HSCs found in the bone marrow of recipient mice was the same for both genotypes, when measured 16 h after transplantation (Figures S7A and S7B). The *Pole3*<sup>m3/m3</sup> mutant bone marrow preferentially gives rise to myeloid cells compared with wild-type progenitors (Figure 5C). The failing reconstitution of both B and T compartments in the recipient mice (Figures 5D and 5E) essentially recapitulates the phenotype in *Pole3*<sup>m3/m3</sup> mice and provides strong support for the notion that the stromal microenvironment in the primary lymphoid organs contributes little, if anything, to the observed pathology. Impaired hematopoietic reconstitution by *Pole3*<sup>m3/m3</sup> progenitor cells is mirrored in the composition of lymphocyte populations in primary and secondary lymphoid organs, respectively. At 16 weeks after transplantation, wild-type CD45.2 and CD45.1 competitor cells contributed equally well to T cell development in the thymus of recipient mice, whereas *Pole3*<sup>m3/m3</sup> mutant hematopoietic progenitors failed to repopulate the recipients (Figure 5F). However, whereas the contributions of *Pole3*<sup>m3/m3</sup> donor cells to DN1, DN2, and DN3 stages are about 10-fold lower than wild-type competitors, the contribution of the *Pole3*<sup>m3/m3</sup> cells to later stages of T cell differentiation falls precipitously and is 2 orders of magnitude lower than that of wild-type cells from the DP stage onward (Figures 5F and S7C). Accordingly, only small numbers of mature *Pole3*<sup>m3/m3</sup>-derived CD4<sup>+</sup> and CD8<sup>+</sup> T cells are found in the spleen and lymph nodes (Figures 5G, 5H, and S7D). Similar to the situation in *Pole3*<sup>m3/m3</sup> mice, T cell defects were restricted to the  $\alpha\beta$  lineage, whereas  $\gamma\delta$  T cell numbers were only mildly reduced in the periphery (Figures 5G and 5H), again indicative

(C) Cartoon illustrating the developmental stages of B cell differentiation in the bone marrow. The dotted line depicts the differentiation block observed in *Pole3*<sup>m3/m3</sup> mice. imm., immature B cells; re-circ., re-circulating B cells.



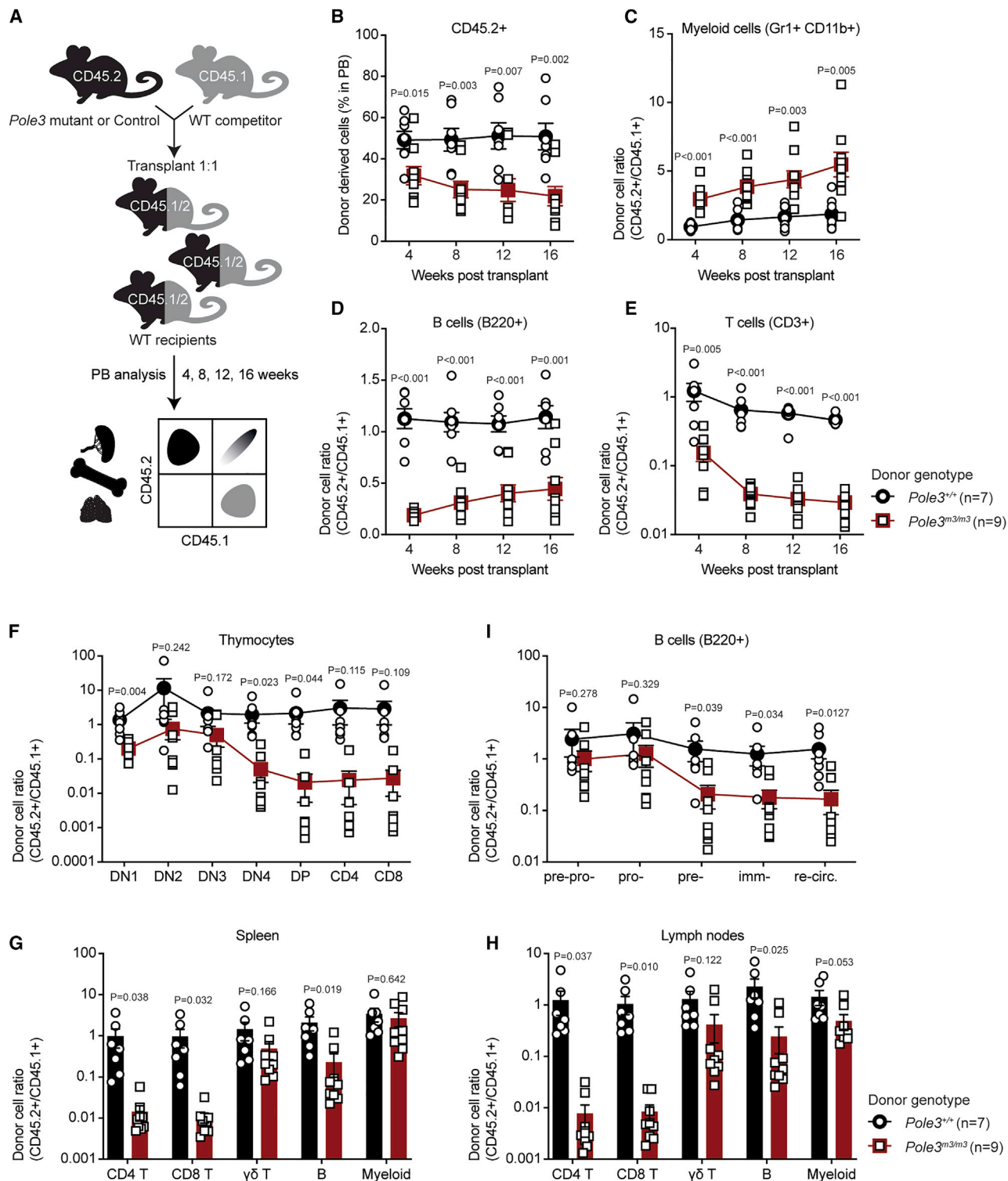


**Figure 5. Pole3 Acts in a Cell-Autonomous and Cell Type-Specific Manner during Lymphocyte Development**

(A) Schematic outline of the competitive transplantation assay. Wild-type competitors exhibit the CD45.1 allotype, whereas *Pole3*<sup>+/+</sup> and *Pole3*<sup>m3/m3</sup> test cells are of CD45.2 allotype. Lethally irradiated CD45.1<sup>+</sup>/CD45.2<sup>+</sup> heterozygous mice served as recipients. The extent of peripheral blood (PB) reconstitution was serially analyzed at 4, 8, 12, and 16 weeks after transplantation. At 16 weeks, the recipient mice were sacrificed, and lymphoid organs were analyzed for lineage reconstitution.

(B) Frequency of donor-derived cells (CD45.1<sup>+</sup> and CD45.2<sup>+</sup>) in peripheral blood of recipient mice.

(legend continued on next page)

of a stronger propensity of *Pole3*<sup>m3/m3</sup> progenitors to complete the  $\gamma\delta$  T cell differentiation pathway.

The pattern of B cell differentiation of *Pole3*<sup>m3/m3</sup> donor cells in wild-type recipients closely mimicked the phenotype of *Pole3*<sup>m3/m3</sup> mice, as illustrated by a drastically reduced contribution of mutant cells to cell types emerging from pre-pro- and pro-B cell progenitor populations in the bone marrow (Figures 5I and S7E), resulting in reduced numbers of B cells in peripheral lymphoid organs (Figures 5G, 5H, and S7D). Collectively, our studies indicate that the hematopoietic phenotype observed in *Pole3*<sup>m3/m3</sup> mice is cell intrinsic.

As a result of peripheral lymphopenia, a greater fraction of *Pole3*<sup>m3/m3</sup> T cells exhibit the surface phenotype of activated/effector cells (CD44<sup>+</sup>CD62L<sup>-</sup>), with a corresponding reduction of naive cells (CD44<sup>+</sup>CD62L<sup>+</sup>) (Figures 6A–6C). *In vitro* stimulation of carboxyfluorescein succinimidyl ester (CFSE)-labeled TCR- $\beta$ <sup>+</sup>CD8<sup>+</sup> splenocytes with a combination of anti-CD3 and anti-CD28 antibodies showed that mutant cells were largely similar in their response profile to wild-type cells (Figure 6D), indicating that *Pole3*<sup>m3/m3</sup> CD8<sup>+</sup> T cells are well capable of proliferating upon TCR-dependent activation. This observation again indicates that mutant cells can attain a differentiated state and respond to physiological proliferative stimuli.

### The *Pole3* Mutation Interferes with Cell Cycle Progression during T Cell Development

POLE is one of the two major DNA replicases with a peak in activity during the S-phase of the cell cycle (Langston et al., 2014; Navas et al., 1995). In order to examine whether and how cell division is affected in actively dividing cells of the *Pole3*<sup>m3/m3</sup> genotype, we first turned to primary cells and analyzed the cell cycle of adult lung fibroblasts (ALFs). No significant differences in cell cycle progression were observed between wild-type and mutant ALFs, as indicated by the analysis of EdU incorporation and DNA content (Figures 7A and 7B). This finding strongly reinforces the notion that, in contrast to POLE1, POLE3 is not essential for cell proliferation.

Inhibition of cell cycle proteins selectively affects the differentiation of the  $\alpha\beta$  T cell lineage; to explain this phenomenon, it was proposed that cell differentiation and proliferation may not always exhibit an antagonistic relationship (Kreslavsky et al., 2012). Because the phenotype of mice described here resembles this particular constellation, we examined the cell cycle dynamics in developing  $\alpha\beta$  thymocytes of mutant *Pole3* mice. For the *in vivo* analysis in adult mice, EdU incorporation was determined by flow cytometry at all stages of intrathymic T cell differentiation. In contrast to controls, fewer *Pole3*<sup>m3/m3</sup> thymocytes are in early S-phase, and more cells are found within the fraction with high

levels of EdU incorporation, indicative of late S-phase cells (Figure 7C). This phenotype suggests that mutant cells progress through the S-phase faster than their wild-type counterparts; this phenotype is particularly pronounced within the DN3, DN4, and DP T cell compartments (Figure 7D). Thymocytes of *Pole3* mutants do not suffer increased DNA damage, as shown by the normal levels of H2AX histone phosphorylation (Figure S7F). Collectively, mice homozygous for mutant alleles of *Pole3* exhibit changes in cell cycle dynamics for some but not all cell types, and these changes seem to be unrelated to the ataxia telangiectasia and Rad3-related (ATR) kinase-pH2AX DNA damage response.

### DISCUSSION

The POLE holoenzyme is essential for DNA replication. Yet not all germline mutations in the gene encoding the catalytic subunit of the enzyme POLE1 or the second essential component POLE2 are lethal, pointing to the presence of compensatory mechanisms (Zhou et al., 2019) and additional non-replicative functions of the holoenzyme complex. Indeed, human syndromes associated with POLE mutations were discovered that present with tissue-specific aberrations, including immunodeficiency (Frugoni et al., 2016; Logan et al., 2018; Pachlopnik Schmid et al., 2012), although the mechanism(s) by which this tissue specificity arises from a ubiquitously required complex have remained obscure. Here, we have addressed this problem by focusing on possible cell-type-specific roles of one of the two small subunits of the complex, POLE3 and POLE4. Several features of POLE3 suggest that this subunit as a likely candidate for a link between replicative and non-replicative functions of the POLE complex. First, POLE3 appears to be a component of chromatin remodeling complexes (Kukimoto et al., 2004; Poot et al., 2000), hinting at possible non-replicative functions. Moreover, deletion of the C terminus of POLE3 does not interfere with the binding of the hAFC1-SNF2H chromatin remodeling complex (Figure 7E), suggesting that this binding is mediated by aa residues 1–100 (Kukimoto et al., 2004). In addition, POLE3 and POLE4 form heterodimers through interaction of their histone fold domains, independent of the other two complex components (Li et al., 2000), and may thus participate also in other molecular contexts. Indeed, as the interaction sites of hAFC1-SNF2H and POLE4 overlap, it is likely that the cellular pool of POLE3 is part of functionally distinct protein complexes (POLE3/hAFC1-SNF2H and POLE3/POLE4, respectively). Finally, POLE3 possesses an evolutionarily conserved C terminus rich in negatively charged amino acids that is absent from POLE4 and may serve to mediate and/or to modulate complex formation, as demonstrated here.

(C) Contributions of donor cells to the myeloid cell compartment.

(D) Contributions of donor cells to the B cell compartment.

(E) Contributions of donor cells to the T cell compartment.

(F) Contributions of donor cells to the various stages of T cell development in the thymus.

(G) Contributions of donor cells to the hematopoietic compartment in the spleen.

(H) Contributions of donor cells to the hematopoietic compartment in the lymph nodes.

(I) Contributions of donor cells to the various stages of B cell development in the bone marrow.

In (C)–(I), the ratios of CD45.2<sup>+</sup> (wild-type or mutant) cells to CD45.1<sup>+</sup> competitor cells are shown. In (B)–(I), mean  $\pm$  SEM is indicated; wild-type and homozygous mutant donors are compared (p values of t tests are indicated); each data point represents one mouse. imm., immature B cells; re-circ., re-circulating B cells.

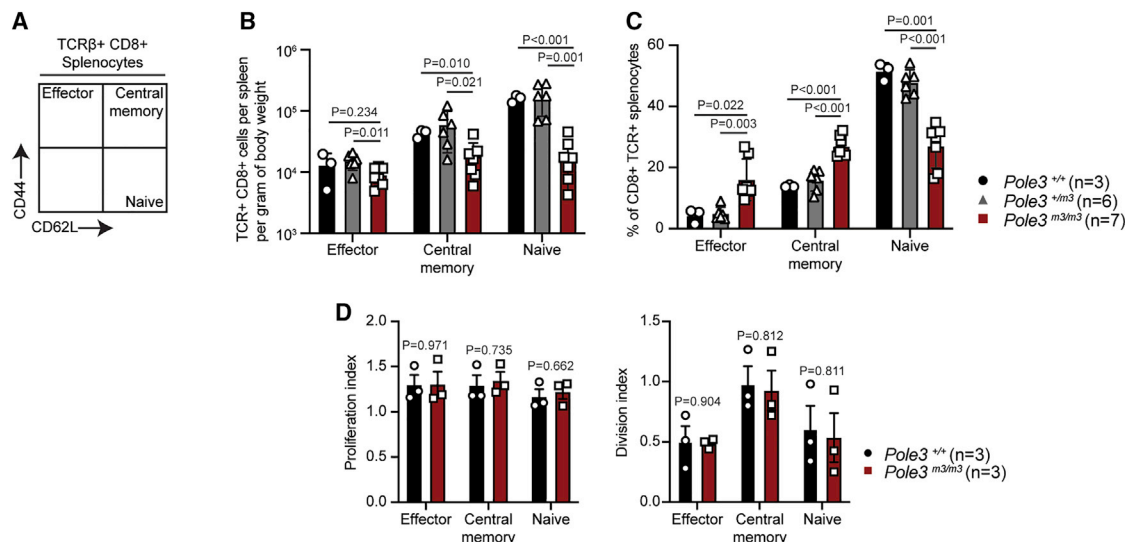


**Figure 6. Characterization of Peripheral T Cell Subsets**

(A) Gating strategy for analysis of CD8<sup>+</sup> T cell populations in the spleen of adult mice.

(B and C) Total numbers (B) and frequencies (C) of effector (CD44<sup>+</sup>CD62L<sup>-</sup>), central memory (CD44<sup>+</sup>CD62L<sup>+</sup>), and naive (CD44<sup>-</sup>CD62L<sup>+</sup>) CD8<sup>+</sup> T cell populations in the spleen of mice with the indicated genotypes.

(D) Analysis of proliferation capacity of CD8<sup>+</sup> T cells isolated from the spleen as determined by CFSE dilution following stimulation with antibodies against CD3 and CD28. Proliferation (left panel) and division indices (right panel) are shown. Bar graphs indicate mean ± SEM; p values of pairwise comparisons by t test are shown; each data point represents one mouse.

In tissue culture cells, the C terminus of POLE3 was shown to be required for replication-dependent nucleosome remodeling through the interaction with the histones H3 and H4 (Bellelli et al., 2018a). However, unexpectedly, we observed no deleterious phenotype in mice homozygous for the *Pole3*ΔC mutant, pointing to the presence of a compensation mechanism, which can buffer such ill effects in the organismal context but not in tissue culture. A different experimental strategy was therefore required to overcome such compensatory mechanism(s) and to be able to examine the role of the C terminus in POLE3-containing complexes other than POLE3/H3-H4. When the predominantly negatively charged tail was converted to positively charged versions, a non-redundant function of this domain for lymphocyte development was revealed. Because deletion of the entire C terminus has no effect on lymphocyte development, we conclude that the neomorphic alleles counteract the function of POLE3 in a distinct protein complex, wherein a lymphocyte stage-specific factor(s) binds to the N-terminal half of the protein (aa 1–96). Because of the lack of a specific *Pole3* antibody that recognizes the N-terminal domain of the protein, it was not possible to directly demonstrate the presence of the mutant proteins. However, the distinct phenotypes observed in our mouse lines strongly argue that the neomorphic alleles give rise to appreciable amounts of mutant proteins.

The rapid progression through the S-phase in our *Pole3* mutant thymocytes is in line with the observation that the *Pole3* yeast homolog (Dpb4) controls the activation of the S-phase checkpoint under conditions of replication stress (Puddu et al., 2011). Moreover, the fact that changes in *Pole3* function are associated with increased sensitivity to ATR kinase inhibition (Hustedt et al., 2019) suggests that in addition to the ATR pathway, a *Pole3*-dependent mode of cell cycle regulation ex-

ists. Our results suggest that the latter is particularly important in the lymphoid lineage.

Our study shows that the arrest of lymphocyte differentiation occurs at equivalent stages during T and B cell development in *Pole3* mutant mice. This suggests that the non-replicative activity of POLE3 targets a component(s) shared by the two principal lymphocyte lineages, which becomes functionally critical at the DN3 stage of T cell differentiation and at the pre-B cell stage in B cell development. From an evolutionary perspective, this suggests that POLE3 became incorporated into the genetic network directing the differentiation of lymphocyte-like cells already in the common ancestor of vertebrates, and possibly even earlier. This functional requirement was maintained at early stages of vertebrate evolution during the time when the two principal lymphocyte lineages emerged and assumed their different functions in the adaptive immune system. The emergence of a novel interaction partner for POLE3 may have been accompanied by subtle modifications in the protein sequence of POLE3 itself, so that it could maintain its replicative function while expanding the range of participation in cell-type-specific protein complexes.

In summary, we have identified the POLE3 subunit of the POLE holoenzyme as a multi-functional protein that connects the replicative function of the POLE holoenzyme and a non-replicative activity in lymphocytes. We anticipate that more immunodeficiency syndromes will be discovered that can be linked to such non-canonical functions of large protein complexes.

## STAR★METHODS

Detailed methods are provided in the online version of this paper and include the following:

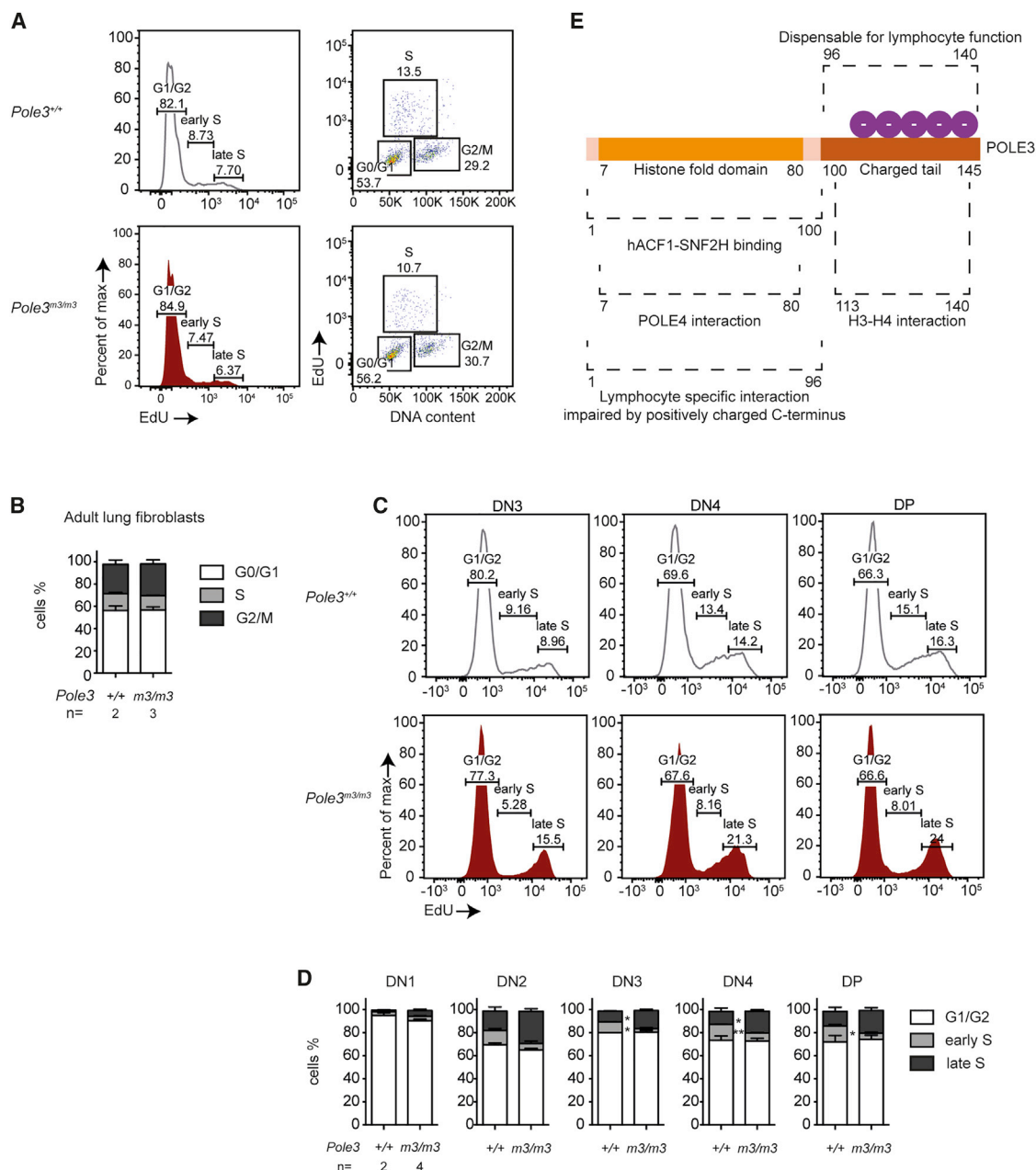


**Figure 7. The *Pole3* Mutation Interferes with Cell Cycle Progression during T Cell Development**

(A) Representative cell cycle profiles of adult lung fibroblasts (ALFs) isolated from *Pole3*<sup>+/+</sup> and *Pole3*<sup>m3/m3</sup> mice. EdU intensity increases with progression through the S-phase of the cell cycle (left panels). The cell cycle stages are characterized by their EdU incorporation and DNA content profiles (right panels): G0/G1 phase (EdU-negative, 2n DNA content), S phase (EdU-positive, 2n to 4n DNA content), and G2/M phase (EdU-negative, 4n DNA content).

(B) Quantification of cell cycle profiles of ALFs is shown. Bar graphs indicate mean  $\pm$  SEM.

(C) Representative histograms of EdU incorporation of indicated thymocyte populations in adult mice of the indicated genotypes.

(D) Quantification of cell cycle stages for the indicated stages of thymocytes. Bar graphs indicate mean  $\pm$  SEM. Significance levels as determined by t test are indicated: \* $p < 0.05$  and \*\* $p < 0.002$ .

(E) Schematic representation of interaction surfaces of POLE3 proteins. The N-terminal region of the protein (1–100 aa) was shown to interact with the human nucleosome sliding complex hACF1-SNF2H and with POLE4. The C-terminal domain (96–145 aa) was shown to interact with a complex composed of histones H3-H4 in tissue culture cells but is dispensable for lymphocyte development *in vivo*. Lymphocyte-specific protein interactions of Pole3 are abolished when the negative charge of the C terminus is converted to a positive charge.



- **KEY RESOURCES TABLE**
- **RESOURCE AVAILABILITY**
  - Lead Contact
  - Materials Availability
  - Data and Code Availability
- **EXPERIMENTAL MODEL AND SUBJECT DETAILS**
  - Mice
- **METHOD DETAILS**
  - CRISPR-Cas9 mediated gene editing in the mouse
  - Alcian Blue/Alizarin Red staining
  - Flow cytometry and cell sorting
  - Annexin V apoptosis detection in developing lymphocytes
  - Semiquantitative RT-PCR
  - Immunoblotting
  - ELISA Immunoassay for serum Immunoglobulins
  - Immunofluorescence staining of frozen spleen sections
  - Adult Lung Fibroblast (ALF) isolation and short-term *in vitro* culture
  - EdU staining and cell cycle analysis
  - CFSE cell proliferation assay of sorted CD8<sup>+</sup> T cell populations
  - Competitive bone marrow reconstitution
  - Analysis of TCR $\beta$  rearrangements
  - Image processing
- **QUANTIFICATION AND STATISTICAL ANALYSIS**

## SUPPLEMENTAL INFORMATION

Supplemental Information can be found online at <https://doi.org/10.1016/j.celrep.2020.107756>.

## ACKNOWLEDGMENTS

We are grateful to Benoît Kanzler for help with the generation of *Pole3* mutant mice; to Ingrid Fidler and Dagmar Diekhoff for animal husbandry; and to Michael Schorpp, Jeremy Swann, Hanspeter Pircher, and Klaus Schwarz for helpful discussion and advice. These studies were supported by the Max Planck Society and the European Research Council (ERC) under the European Union's Seventh Framework Programme (FP7/2007-2013), ERC grant agreement 323126. I.S. is a member of the International Max Planck Research School, a joint graduate program between the Max Planck Institute of Immunobiology and Epigenetics and the University of Freiburg.

## AUTHOR CONTRIBUTIONS

I.S., N.I., T.C., and C.P.O. performed the experiments. I.S., N.I., T.C., E.T., C.P.O., and T.B. designed the experiments and analyzed the data. I.S. and T.B. wrote the paper. All authors commented on the manuscript. T.B. coordinated the design and implementation of the study.

## DECLARATION OF INTERESTS

The authors declare no competing interests.

Received: October 14, 2019

Revised: April 6, 2020

Accepted: May 20, 2020

Published: June 16, 2020

## REFERENCES

- Araki, H., Hamatake, R.K., Johnston, L.H., and Sugino, A. (1991a). DPB2, the gene encoding DNA polymerase II subunit B, is required for chromosome replication in *Saccharomyces cerevisiae*. *Proc. Natl. Acad. Sci. U S A* **88**, 4601–4605.
- Araki, H., Hamatake, R.K., Morrison, A., Johnson, A.L., Johnston, L.H., and Sugino, A. (1991b). Cloning DPB3, the gene encoding the third subunit of DNA polymerase II of *Saccharomyces cerevisiae*. *Nucleic Acids Res.* **19**, 4867–4872.
- Bamezai, A., Palliser, D., Berezovskaya, A., McGrew, J., Higgins, K., Lacy, E., and Rock, K.L. (1995). Regulated expression of Ly-6A.2 is important for T cell development. *J. Immunol.* **154**, 4233–4239.
- Bellelli, R., Belan, O., Pye, V.E., Clement, C., Maslen, S.L., Skehel, J.M., Cherpanov, P., Almouzni, G., and Boulton, S.J. (2018a). POLE3-POLE4 is a histone H3-H4 chaperone that maintains chromatin integrity during DNA replication. *Mol. Cell* **72**, 112–126.e5.
- Bellelli, R., Borel, V., Logan, C., Svendsen, J., Cox, D.E., Nye, E., Metcalfe, K., O'Connell, S.M., Stamp, G., Flynn, H.R., et al. (2018b). Polepsilon instability drives replication stress, abnormal development, and tumorigenesis. *Mol. Cell* **70**, 707–721.e7.
- Frugoni, F., Dobbs, K., Felgentreff, K., Aldhekri, H., Al Saud, B.K., Amaout, R., Ali, A.A., Abhyankar, A., Alroqi, F., Gillani, S., et al. (2016). A novel mutation in the POLE2 gene causing combined immunodeficiency. *J. Allergy Clin. Immunol.* **137**, 635–638.e1.
- Grawunder, U., Zimmer, D., Fugmann, S., Schwarz, K., and Lieber, M.R. (1998). DNA ligase IV is essential for V(D)J recombination and DNA double-strand break repair in human precursor lymphocytes. *Mol. Cell* **2**, 477–484.
- Henderson, S.C., and Bamezai, A. (2003). Loss of Ly-6A.2 expression on immature developing T cells in the thymus is necessary for their normal growth and generation of the Vbeta T-cell repertoire. *Tissue Antigens* **62**, 117–132.
- Hustedt, N., Álvarez-Quijón, A., McEwan, A., Yuan, J.Y., Cho, T., Koob, L., Hart, T., and Durocher, D. (2019). A consensus set of genetic vulnerabilities to ATR inhibition. *Open Biol.* **9**, 190156.
- Hwang, W.Y., Fu, Y., Reyon, D., Maeder, M.L., Tsai, S.Q., Sander, J.D., Peterson, R.T., Yeh, J.R., and Joung, J.K. (2013). Efficient genome editing in zebrafish using a CRISPR-Cas system. *Nat. Biotechnol.* **31**, 227–229.
- Jaszczur, M., Flis, K., Rudzka, J., Kraszewska, J., Budd, M.E., Polaczek, P., Campbell, J.L., Jonczyk, P., and Fijalkowska, I.J. (2008). Dpb2p, a noncatalytic subunit of DNA polymerase epsilon, contributes to the fidelity of DNA replication in *Saccharomyces cerevisiae*. *Genetics* **178**, 633–647.
- Kawamoto, H., Ikawa, T., Ohmura, K., Fujimoto, S., and Katsura, Y. (2000). T cell progenitors emerge earlier than B cell progenitors in the murine fetal liver. *Immunity* **12**, 441–450.
- Kreslavsky, T., Gleimer, M., Miyazaki, M., Choi, Y., Gagnon, E., Murre, C., Sincinski, P., and von Boehmer, H. (2012).  $\beta$ -Selection-induced proliferation is required for  $\alpha\beta$  T cell differentiation. *Immunity* **37**, 840–853.
- Kukimoto, I., Elderkin, S., Grimaldi, M., Oelgeschläger, T., and Varga-Weisz, P.D. (2004). The histone-fold protein complex CHRAC-15/17 enhances nucleosome sliding and assembly mediated by ACF. *Mol. Cell* **13**, 265–277.
- Kunkel, T.A., and Burgers, P.M. (2008). Dividing the workload at a eukaryotic replication fork. *Trends Cell Biol.* **18**, 521–527.
- Langston, L.D., Zhang, D., Yurieva, O., Georgescu, R.E., Finkelstein, J., Yao, N.Y., Indiani, C., and O'Donnell, M.E. (2014). CMG helicase and DNA polymerase  $\epsilon$  form a functional 15-subunit holoenzyme for eukaryotic leading-strand DNA replication. *Proc. Natl. Acad. Sci. U S A* **111**, 15390–15395.
- Li, Y., Pursell, Z.F., and Linn, S. (2000). Identification and cloning of two histone fold motif-containing subunits of HeLa DNA polymerase epsilon. *J. Biol. Chem.* **275**, 23247–23252.
- Logan, C.V., Murray, J.E., Parry, D.A., Robertson, A., Bellelli, R., Tarnauskaitė, Ž., Challis, R., Cleal, L., Borel, V., Fluteau, A., et al.; SGP Consortium (2018). DNA polymerase epsilon deficiency causes IMAGe syndrome with variable immunodeficiency. *Am. J. Hum. Genet.* **103**, 1038–1044.

- Mombaerts, P., Iacomini, J., Johnson, R.S., Herrup, K., Tonegawa, S., and Papaioannou, V.E. (1992). RAG-1-deficient mice have no mature B and T lymphocytes. *Cell* 68, 869–877.
- Moshous, D., Callebaut, I., de Chasseval, R., Corneo, B., Cavazzana-Calvo, M., Le Deist, F., Tezcan, I., Sanal, O., Bertrand, Y., Philippe, N., et al. (2001). Artemis, a novel DNA double-strand break repair/V(D)J recombination protein, is mutated in human severe combined immune deficiency. *Cell* 105, 177–186.
- Navas, T.A., Zhou, Z., and Elledge, S.J. (1995). DNA polymerase epsilon links the DNA replication machinery to the S phase checkpoint. *Cell* 80, 29–39.
- O'Driscoll, M., Cerosaletti, K.M., Girard, P.M., Dai, Y., Stumm, M., Kysela, B., Hirsch, B., Gennery, A., Palmer, S.E., Seidel, J., et al. (2001). DNA ligase IV mutations identified in patients exhibiting developmental delay and immunodeficiency. *Mol. Cell* 8, 1175–1185.
- Ohya, T., Maki, S., Kawasaki, Y., and Sugino, A. (2000). Structure and function of the fourth subunit (Dpb4p) of DNA polymerase epsilon in *Saccharomyces cerevisiae*. *Nucleic Acids Res.* 28, 3846–3852.
- Oxenius, A., Bachmann, M.F., Zinkernagel, R.M., and Hengartner, H. (1998). Virus-specific MHC-class II-restricted TCR-transgenic mice: effects on humoral and cellular immune responses after viral infection. *Eur. J. Immunol.* 28, 390–400.
- Pachlopnik Schmid, J., Lemoine, R., Nehme, N., Cormier-Daire, V., Revy, P., Debeurme, F., Debré, M., Nitschke, P., Bole-Feysot, C., Legeai-Mallet, L., et al. (2012). Polymerase  $\epsilon$ 1 mutation in a human syndrome with facial dysmorphism, immunodeficiency, livedo, and short stature ("FILS syndrome"). *J. Exp. Med.* 209, 2323–2330.
- Poot, R.A., Dellaire, G., Hülsmann, B.B., Grimaldi, M.A., Corona, D.F., Becker, P.B., Bickmore, W.A., and Varga-Weisz, P.D. (2000). HuCHRA, a human ISWI chromatin remodelling complex contains hACF1 and two novel histone-fold proteins. *EMBO J.* 19, 3377–3387.
- Puddu, F., Piergiovanni, G., Plevani, P., and Muzi-Falconi, M. (2011). Sensing of replication stress and Mec1 activation act through two independent pathways involving the 9-1-1 complex and DNA polymerase  $\epsilon$ . *PLoS Genet.* 7, e1002022.
- Puel, A., Ziegler, S.F., Buckley, R.H., and Leonard, W.J. (1998). Defective IL7R expression in T(-)B(+)NK(+) severe combined immunodeficiency. *Nat. Genet.* 20, 394–397.
- Rigueur, D., and Lyons, K.M. (2014). Whole-mount skeletal staining. *Methods Mol. Biol.* 1130, 113–121.
- Schwarz, K., Gauss, G.H., Ludwig, L., Pannicke, U., Li, Z., Lindner, D., Friedrich, W., Seger, R.A., Hansen-Hagge, T.E., Desiderio, S., et al. (1996). RAG mutations in human B cell-negative SCID. *Science* 274, 97–99.
- Tramont, P.C., Tosello-Tramont, A.C., Shen, Y., Duley, A.K., Sutherland, A.E., Bender, T.P., Littman, D.R., and Ravichandran, K.S. (2010). CXCR4 acts as a costimulator during thymic beta-selection. *Nat. Immunol.* 11, 162–170.
- van der Burg, M., Ijspeert, H., Verkaik, N.S., Turul, T., Wiegant, W.W., Morotomi-Yano, K., Mari, P.O., Tezcan, I., Chen, D.J., Zdzienicka, M.Z., et al. (2009). A DNA-PKcs mutation in a radiosensitive T-B- SCID patient inhibits Artemis activation and nonhomologous end-joining. *J. Clin. Invest.* 119, 91–98.
- Woodbine, L., Neal, J.A., Sasi, N.K., Shimada, M., Deem, K., Coleman, H., Dobyns, W.B., Ogi, T., Meek, K., Davies, E.G., and Jeggo, P.A. (2013). PRKDC mutations in a SCID patient with profound neurological abnormalities. *J. Clin. Invest.* 123, 2969–2980.
- Zhou, Z.X., Lujan, S.A., Burkholder, A.B., Garbacz, M.A., and Kunkel, T.A. (2019). Roles for DNA polymerase  $\delta$  in initiating and terminating leading strand DNA replication. *Nat. Commun.* 10, 3992.

## STAR★METHODS

### KEY RESOURCES TABLE

REAGENT or RESOURCE	SOURCE	IDENTIFIER
<b>Antibodies</b>		
CD4 APC Cy7 Clone GK1.5	Biolegend	Cat#100414
CD8a PE Clone 53-6.7	eBioscience	Cat#12-0081-85
CD44 APC Clone IM7	eBioscience	Cat#17-0441-81
CD25 PE Cy7 Clone PC61	BD Biosciences	Cat#552880
B220 (CD45R) FITC Clone RA3-6B2	Biolegend	Cat#103206
TCR $\gamma\delta$ FITC Clone eBioGL3	eBioscience	Cat#11-5711-82
NK1.1 FITC Clone PK136	Biolegend	Cat#108706
CD11c FITC Clone HL3	BD Biosciences	Cat#557400
CD11b (Mac1) FITC Clone M1/70	BD Biosciences	Cat#557396
CD4 PE Dazzle Clone GK1.5	Biolegend	Cat#100455
CD8a BV421 Clone 53-6.7	Biolegend	Cat#100738
TCR $\gamma\delta$ PerCP Cy5.5 Clone GL3	Biolegend	Cat#118118
B220 (CD45R) PE Clone RA3-6B2	Biolegend	Cat#103208
NK1.1 PE Clone PK136	eBioscience	Cat#12-5941-83
CD11c PE Clone N418	eBioscience	Cat#12-0114-82
CD11b (Mac1) PE Clone M1/70	BD Biosciences	Cat#553311
TCR- $\beta$ PE Clone H57-597	eBioscience	Cat#12-5961-83
CXCR4 (CD184) PE Clone L276F12	Biolegend	Cat#146506
CD44 PE Clone IM7	BD Biosciences	Cat#553134
CD25 Alexa Fluor® 647 Clone PC61	Biolegend	Cat#102020
Sca1 (Ly-6A/E) PE Cy7 Clone D7	Biolegend	Cat#108113
IgM FITC Clone II/41	BD Biosciences	Cat#553437
BP-1 (Ly51) PE Clone 6C3	Thermo Fischer	Cat#12-5891-83
CD43 APC Clone S7	BD Biosciences	Cat#560663
B220 (CD45R) PE Cy7 Clone RA3-6B2	eBioscience	Cat#25-0452-82
CD24 eFluor® 450 Clone M1/69	eBioscience	Cat#48-0242-82
IgM PE Clone II/41	eBioscience	Cat#12-5790-81
CD3 PerCP Cy5.5 Clone 145-2C11	Biolegend	Cat#100328
CD3 PE Clone 145-2C11	Biolegend	Cat#100308
Fas (CD95) APC Clone SA367H8	Biolegend	Cat#152603
GL7 BV421 Clone GL7	BD Biosciences	Cat#562967
IgM eFluor® 450 Clone II/41	eBioscience	Cat#48-5790-82
IgD Alexa Fluor® 647 Clone 11-26c.2a	Biolegend	Cat#405707
GL7 Alexa Fluor® 488 Clone GL7	Biolegend	Cat#144612
B220 (CD45R) Alexa Fluor® 647 Clone RA3-6B2	BD Biosciences	Cat#557683
CD169 (Siglec-1) BV421 Clone 3D6.112	Biolegend	Cat#142421
CD25 BV605 Clone PC61	Biolegend	Cat#102035
CD8a PE Clone 53-6.7 Cy7	eBioscience	Cat#25-0081-82
CD4 PE Dazzle Clone GK1.5	Biolegend	Cat#100455
TCR $\beta$ BV421 Clone H57-597	Biolegend	Cat#109229
CD62L Alexa Fluor® 700 Clone MEL-14	Biolegend	104426

(Continued on next page)

**Continued**

REAGENT or RESOURCE	SOURCE	IDENTIFIER
CD44 APC Clone IM7	eBioscience	Cat#17-0441-81
CD19 PE Clone eBio1D3	eBioscience	Cat#12-0193-83
CD3e FITC Clone 145-2C11	Biolegend	Cat#100306
Gr1 (Ly-6G/Ly-6C) FITC Clone RB6-8C5	Biolegend	Cat#108406
TER-119 FITC Clone TER-119	eBioscience	Cat#11-5921-81
Sca1 (Ly-6A/E) APC Clone D7	eBioscience	Cat#17-5981-81
Ckit (CD117) BV421 Clone 2B8	Biolegend	Cat#105827
Fli2 (CD135) PE Clone A2F10.1	BD Biosciences	Cat#561068
CD34 Alexa Fluor® 700 Clone RAM34	eBioscience	Cat#56-0341-82
CD150 (SLAMF) BV605 Clone TC15-12F12.2	Biolegend	Cat#115927
CD48 APC Cy7 Clone HM48-1	Biolegend	Cat#103431
IL-7Ra PE Dazzle Clone A7R34	Biolegend	Cat#135031
Fli2 (CD135) PerCP efluor710 Clone A2F10	eBioscience	Cat#46-1351-80
CD45.1 PE Clone A20	eBioscience	Cat#12-0453-83
CD45.2 BV421 Clone 104	Biolegend	Cat#109831
CD3e APC Clone 145-2C11	Thermo Fischer	Cat#17-0031-82
CD48 PerCP efluor710 Clone HM48-1	eBioscience	Cat#46-0481-82
CD150 (SLAMF) PE Dazzle Clone TC15-12F12.2	Biolegend	Cat#115935
CD45.2 Alexa Fluor® 700 Clone 104	Biolegend	Cat#109822
CD45.1 APC Cy7 Clone A20	Biolegend	Cat#110716
CD4 PE Cy7 Clone GK1.5	Biolegend	Cat#100422
CD43 PE Clone S7	BD Biosciences	Cat#553271
Gr1 (Ly-6G/Ly-6C) PE Clone RB6-8C5	Biolegend	Cat#108408
γH2AX (phospho-Ser139) mouse monoclonal antibody (clone JBW301)	Millipore	Cat#05-636, RRID:AB_309864
Pan-actin rabbit polyclonal antibody	Sigma	Cat#A2066, RRID:AB_476693
Goat anti-rabbit Immunoglobulins/ HRP	Agilent Dako	Cat#P0448,
Goat anti-mouse Immunoglobulins/ HRP	Agilent Dako	Cat#P0447
<b>Chemicals, Peptides, and Recombinant Proteins</b>		
3',6'-dihydroxy-3-oxo-spiro [isobenzofuran-1(3H),9'-[9H]xanthene]-5-carboxylic acid, 2,5-dioxo-1-pyrrolidinyl ester (CFSE)	Cayman Chemicals	Cat#16802
Recombinant Cas9 Protein	PNA Bio Inc	Cat#CP01
α-GalCer Loaded CD1 tetramer PE	ProImmune	Cat#E001-2X
<b>Critical Commercial Assays</b>		
Click-iT EdU Flow Cytometry Assay, Alexa Fluor 488 dye	Thermo Fisher	Cat#C10337
FoxP3/Transcription staining buffer set	eBioscience	Cat#00-5523-00
Superscript II Reverse Transcription	Thermo Fischer	Cat#18064022
IgM Mouse Uncoated ELISA Kit	Thermo Fischer	Cat#88-50470
IgG (Total) Mouse Uncoated ELISA Kit	Thermo Fischer	Cat#88-50400
IgG1 Mouse Uncoated ELISA Kit	Thermo Fischer	Cat#88-50410
IgG2b Mouse Uncoated ELISA Kit	Thermo Fischer	Cat#88-50430
IgG2c Mouse Uncoated ELISA Kit	Thermo Fischer	Cat#88-50670-22
Annexin V Apoptosis Detection Kit FITC	Thermo Fisher	Cat#88-8005-72
<b>Experimental Models: Cell Lines</b>		
Pole3 <sup>tm1(KOMP)Vlcg</sup> ESC line, Clone 12086A-F4	KOMP Repository UC Davis	Strain ID: C57BL/6- Pole3 tm1(KOMP)Vlcg, Design ID: 12086

(Continued on next page)



**Continued**

REAGENT or RESOURCE	SOURCE	IDENTIFIER
<b>Experimental Models: Organisms/Strains</b>		
<i>Pole3<sup>m1</sup></i> , <i>Pole3</i> ENSMUSG00000028394, cDNA c.289-420del, protein p.K97_E140del	this paper	N/A
<i>Pole3<sup>m2</sup></i> , <i>Pole3</i> ENSMUSG00000028394, cDNA c.288-418del, protein p.K97GfsX117	this paper	N/A
<i>Pole3<sup>m3</sup></i> , <i>Pole3</i> ENSMUSG00000028394, cDNA c.294delinsTA, protein p.K100EfsX129	this paper	N/A
<i>Pole3<sup>m4</sup></i> , <i>Pole3</i> ENSMUSG00000028394, cDNA C.297-298insCG, protein p.K100RfsX144	this paper	N/A
<i>Pole3</i> knockout, <i>Pole3</i> ENSMUSG00000028394	this paper, <i>Pole3<sup>tm1(KOMP)Vlcg</sup></i> ESC line from KOMP Repository UC Davis	N/A
<b>Oligonucleotides</b>		
guide RNA sequences (sgRNA) and DNA repair template for CRISPR-Cas9 mutagenesis	this paper, see <a href="#">Table S3</a> for sequences	N/A
Genotyping primers for <i>Pole3</i> mutants and TCRtg	this paper, see <a href="#">Table S4</a> for sequences	N/A
RT-PCR Primers	this paper, see <a href="#">Table S5</a> for sequences	N/A
<b>Recombinant DNA</b>		
DR274 (guide RNA expression vector)	( <a href="#">Hwang et al., 2013</a> )	Addgene plasmid Cat#42250
<b>Software and Algorithms</b>		
FlowJo version 10	FlowJo	<a href="https://www.flowjo.com/solutions/flowjo/downloads">https://www.flowjo.com/solutions/flowjo/downloads</a>
Photoshop CC	Adobe	<a href="https://www.adobe.com">https://www.adobe.com</a>
Illustrator	Adobe	<a href="https://www.adobe.com">https://www.adobe.com</a>
BD FACSDiva 8.0.1	BD Biosciences	<a href="https://www.bdbiosciences.com/us/instruments/clinical/software/flow-cytometry-acquisition/bd-facsddiva-software/facsddiva-software-v-803-win-7-32-bit-os/p/659523">https://www.bdbiosciences.com/us/instruments/clinical/software/flow-cytometry-acquisition/bd-facsddiva-software/facsddiva-software-v-803-win-7-32-bit-os/p/659523</a>
Prism 8	GraphPad	<a href="https://www.graphpad.com/scientific-software/prism/">https://www.graphpad.com/scientific-software/prism/</a>

## RESOURCE AVAILABILITY

### Lead Contact

Further information and requests for resources and reagents should be directed to and will be fulfilled by the Lead Contact, Thomas Boehm ([boehm@ie-freiburg.mpg.de](mailto:boehm@ie-freiburg.mpg.de)).

### Materials Availability

All unique reagents generated in this study are available from the lead Contact with a completed Materials Transfer Agreement. Mouse lines generated in this study are available from the Lead Contact with a completed Materials Transfer Agreement.

### Data and Code Availability

The published article includes all datasets generated or analyzed during this study.

## EXPERIMENTAL MODEL AND SUBJECT DETAILS

### Mice

ES cells carrying a deletion cassette replacing most of the *Pole3* coding sequence were obtained from the KOMP repository and were injected into host blastocysts to generate *Pole3*<sup>-/-</sup> mice under the C57BL/6 genetic background using standard protocols. *Pole3* C-terminal domain mutants (*Pole3*<sup>m1</sup>, *Pole3*<sup>m2</sup>, *Pole3*<sup>m3</sup>, *Pole3*<sup>m4</sup> mutants) were generated by CRISPR-Cas9 technology using recombinant Cas9, sgRNAs and, in one experiment, a sequence-specific single-stranded repair oligonucleotide (listed in Table S3) targeting the last exon of the murine *Pole3* gene, according to standard methods. The deletion in exon 4 was generated by co-injection of two sgRNAs; owing to the presence of a long string of glutamic acid residues in the wild-type protein (Figure 2B) and the similarity of triplets encoding glutamic acid on the one hand (GAA and GAG), and lysine (AAA and AAG) on the other, the imperfect repair processes after Cas9-mediated double-strand breaks generated a variety of mutant alleles by small insertions/deletions, some of which were selected for further study (see Table S3). *Pole3* C-terminal domain mutants were generated on the FVB genetic background and were either kept on that background or were backcrossed to the C57BL/6 strain. Mice expressing a MHC Class II restricted TCR recognizing Lymphocytic Choriomeningitis Virus (LCMV) derived epitope were previously described (Oxenius et al., 1998).

The primers used for mouse genotyping are listed in Table S4. For all experimental procedures, comparisons were made with same-strain littermates in order to exclude strain-specific variations. All mice were kept in the animal facility of the Max Planck Institute of Immunobiology and Epigenetics under conventional housing conditions. All animal experiments were performed in accordance with the relevant guidelines and regulations, approved by the review committee of the Max Planck Institute of Immunobiology and Epigenetics and the Regierungspräsidium Freiburg, Germany (license AZ 35-9185.81/G-15/35).

## METHOD DETAILS

### CRISPR-Cas9 mediated gene editing in the mouse

For gene editing a single guide RNA (sgRNA) approximately 21 nucleotides long was designed complementary to a target site in the genome and was cloned in a pDR274 vector containing a T7 promoter for *in vitro* transcription (sgRNAs listed on Table S3). 15 ng/μl transcribed sgRNA together with 50 ng/ml recombinant Cas9 protein and 5 μM of sequence specific single stranded repair oligo (in case of knock-in gene editing) were mixed together in injection buffer (20 mM Tris HCl pH 7.5, 0.3 mM EDTA in nuclease free ddH<sub>2</sub>O). The mixture was injected into mouse blastocysts and those were transferred into pseudo-pregnant recipient mice; the procedure was carried out in the Transgenic Mouse Core Facility of the MPI-IE. Upon obtaining founder mice (F0), the desired mutations were identified by genotyping.

### Alcian Blue/Alizarin Red staining

Skeletal structures of embryos were revealed by Alcian Blue-Alizarin Red staining (Rigueur and Lyons, 2014). In brief, embryos were collected at 16.5 days post coitum (dpc) and extra-embryonic membranes were removed. After washing in PBS, the embryos were briefly immersed in hot tap water (65°C) and the eyes, skin and internal organs were removed. They were fixed overnight in 95% ethanol at room temperature and then placed in acetone overnight at room temperature to dissolve excess fat. For cartilage staining, the embryos were incubated for 24h in Alcian Blue stain (0.03% Alcian Blue [w/v], 80% EtOH, 20% glacial acetic acid) at room temperature and then destained in two changes of 70% ethanol (4 hours in total), followed by incubation in 95% ethanol overnight. After pre-clearing the embryos with 1% KOH for 1 h, they were immersed in Alizarin Red solution (0.005% Alizarin Red [w/v] in 1% [w/v] KOH) for 4h at room temperature. The embryos were cleared for 24h-36h at 4°C in 50% glycerol, 0.5% (w/v) KOH solution and then transferred to 80% glycerol (in ddH<sub>2</sub>O) for long-term storage. Pictures were taken using a Leica MZ FLII stereomicroscope on a transmitted light base.

### Flow cytometry and cell sorting

Phenotyping of lymphocyte populations was performed by flow cytometry after preparation of single cell suspensions from lymphoid organs and staining using antibodies listed in Table S6. Single cell suspension of thymus, spleen and lymph nodes were prepared in FACS buffer (2% FBS, 1 mM EDTA, 1% penicillin- streptomycin, in PBS) by tissue homogenization with a syringe plunger against a 40 μm cell strainer. For preparation of cell suspensions from bone marrow, femur, tibia and pelvis were flushed with FACS buffer using a 10 mL syringe and a 26 gauge-needle and then passed through 40 μm cell strainer to obtain single cell suspensions. To achieve red blood cell lysis, the cell suspensions were treated with ACK lysis buffer (0.15M NH<sub>4</sub>Cl, 10mM KHCO<sub>3</sub>, 0.1mM EDTA in H<sub>2</sub>O, pH 7.2-7.4), washed and resuspended in FACS buffer. For intracellular staining the cells were first stained with a fixable viability dye prior to surface antibody staining. After cell surface staining the cells were fixed and permeabilized using the FoxP3/Transcription staining buffer set (eBioscience) according to manufacturer's protocol followed by intracellular antibody staining. Data were collected on an LSRFortessa and/or LSRII apparatus (BD Biosciences) and were analyzed with FlowJo software version 10; cell sorting was done using a FACSAria instrument (BD Biosciences).

### **Annexin V apoptosis detection in developing lymphocytes**

The Annexin V (FITC) apoptosis detection Kit (eBioscience) was used for detection of apoptotic cells during development of T and B lymphocytes. Cell suspensions prepared from thymus and bone marrow were first labeled with a viability dye (Fixable viability dye eFluor 780, eBioscience) according to manufacturer's instructions. Then the cells were stained with surface antibodies (listed in [Table S6](#)) in FACS buffer (2% FBS, 1 mM EDTA, 1% penicillin-streptomycin, in PBS). After washing with 1X-diluted Binding Buffer (in dH<sub>2</sub>O) they were resuspended again in 1X Binding Buffer and incubated with FITC-conjugated Annexin V for 15 minutes at room temperature. The cells were finally washed with 1X Binding Buffer and analyzed by flow cytometry.

### **Semiquantitative RT-PCR**

Total RNA was extracted from mouse tissue-derived cells using TriReagent (Sigma Aldrich) following the manufacturer's recommended protocol. To remove genomic DNA, RNA preparations were treated with 1 U of RQ1 RNase-free DNase (Promega) per  $\mu$ g of total RNA in a reaction containing 1X RQ1 RNase-free DNase Reaction buffer. The mixture was incubated at 37°C for 30 minutes. A second round of RNA extraction using TriReagent was performed to remove the DNase from the sample. The quantity and quality of the RNA were assessed by Nanodrop concentration measurement and agarose gel electrophoresis (1.5% agarose gel). For cDNA synthesis the Superscript II Reverse Transcriptase (Thermo Fischer) and oligo(dT1-3) primers were used according to manufacturer's recommended protocol. The obtained cDNA was serially diluted for PCR reactions with Pole3 and phosphoribosyl transferase (Hprt) housekeeping gene primers.

### **Immunoblotting**

For use in western blotting, whole mouse tissue was homogenized and lysed for 15-30 min at 4°C in RIPA lysis buffer (Millipore, Cat#20-188) [50 mM Tris-HCl (pH 7.4), 150 mM NaCl, 1% NP40, 0.25% sodium deoxycholate] supplemented with 0.1% Sodium dodecyl sulfate, protease inhibitor cocktail (Roche, Cat#11836170001) and 1% of each phosphatase inhibitor cocktail 2 and 3 (Sigma, Cat#P5726 and Cat#P0044). Lysates were centrifuged at 18,000xg for 10 min and the supernatant was transferred to a fresh tube prior to snap freezing. Protein lysates were denatured at 95°C in 1X loading buffer (2% SDS w/w, 2mM DTT, 4% Glycine, 0.01% bromophenol blue w/w, 0.04 M Tris pH 6.8, 3%  $\beta$ -mercaptoethanol). SDS-polyacrylamide gel electrophoresis (SDS-PAGE) of heat-denatured protein samples was performed using the NuPAGE SDS-PAGE Gel System and 12% NuPAGE Bis-Tris Precast Gels with MES/SDS running buffer (Thermo Fischer). Blotting to Immuno-Blot PVDF membrane (Biorad) in transfer buffer (25mM Tris, 192mM Glycine, 20% MeOH v/v) was performed for 40 min at 100V using a Mini Trans-Blot Cell Module (Biorad). Membranes were blocked using 5% Bovine Serum Albumin and developed with the following antibodies at dilutions recommended by the manufacturer: anti-phospho Histone H2AX (Ser139), and anti-pan-actin. Membranes were probed with goat  $\alpha$ -rabbit-HRP secondary or goat  $\alpha$ -mouse-HRP secondary antibodies. A chemiluminescent system was used for imaging western blots using ECL Prime Western Blotting Detection Reagents (GE Healthcare) or SuperSignal WestFemto (Thermo Fischer); CX-BL+ X-ray film (AGFA Healthcare) was used for documentation. Contrast and brightness were adjusted for total images using Adobe Photoshop CS6.

### **ELISA Immunoassay for serum Immunoglobulins**

Serum immunoglobulin levels of mice were measured by enzyme-linked immunosorbent assay (ELISA) according to manufacturer's instructions (Invitrogen). Serum was prepared from mouse whole blood and was pre-diluted to be used for ELISA assays. The levels of each immunoglobulin class were expressed as arbitrary unit (AU) per mL serum. These values were interpolated from a standard curve. This curve was generated from a serial dilution of purified mouse immunoglobulin isotype control. One AU corresponds to the OD values obtained with 1  $\mu$ g purified isotype control upon serial dilution.

### **Immunofluorescence staining of frozen spleen sections**

For spleen immunofluorescence staining, frozen spleen sections (8  $\mu$ m) were prepared with a cryostat on Superfrost Plus 25  $\times$  75  $\times$  1 mm microscopy slides (Thermo Fischer). After drying for 20 minutes at room temperature, the sections were surrounded with pap pen and left to dry. The slides were washed for 1 min in PBS and blocked in 1% BSA, 0.2% Tween in PBS for 1 h. The spleen sections were stained with the following fluorescently labeled antibodies at 4°C in a humid chamber in the dark overnight: GL7 Alexa Fluor® 488, CD169 BV421 and B220 Alexa Fluor® 647. The slides were washed three times with PBS and briefly with ddH<sub>2</sub>O. Dried slides were mounted with Fluoromount G (Thermo Fischer). Imaging was done using a LSM780 (Zeiss) microscope and images were processed using Imaris 9.5.1 software (Bitplane). Tiled Immunofluorescent images were stitched together using Zen software (Zeiss). Contrast, brightness and color saturation were adjusted across the entire images using Adobe Photoshop CS6.

### **Adult Lung Fibroblast (ALF) isolation and short-term *in vitro* culture**

For ALF isolation, lungs from euthanized mice were harvested and finely minced with scissors. The lung fragments were digested in 1 mL of digest media (0.2 mg/mL collagenase, 0.2 mg/mL dispase and 2.5  $\mu$ g/mL DNaseI in RPMI 1640, supplemented with 2% FBS and 1 U/mL penicillin- 1  $\mu$ g/mL streptomycin) for 1 h at 37°C. Digestion was stopped by adding 5 mM EDTA, the cells were filtered through a 70  $\mu$ m cell strainer and washed with RPMI 1640 supplemented with 2% FBS (Pan-Biotech) and 1 U/mL penicillin- 1  $\mu$ g/mL streptomycin. Cell suspension was pelleted and resuspended in DMEM (Dulbeccó's modified Eagle's medium) supplemented with 10% FBS and 1 U/mL penicillin- 1  $\mu$ g/mL streptomycin. The cells were plated in T75 flasks (passage 0) and incubated at 37°C with 5% CO<sub>2</sub>. At 70% confluence, the cells were trypsinized, counted and replated on 12-well plates for EdU labeling.

### EdU staining and cell cycle analysis

For *in vivo* cell cycle analysis of thymocytes, mice received a single intra-peritoneal injection of EdU (5-ethynyl-2'-deoxyuridine) diluted in PBS at a dose of 50 mg/kg body weight. After 16h of EdU exposure, the mice were sacrificed and single cell suspensions of thymus were prepared. Single cell suspensions of EdU labeled cells were processed using the Click-iT EdU Flow Cytometry Assay (Thermo Fisher) according to the manufacturers protocol. Briefly, the cells were washed with 1% BSA in PBS and stained with surface antibodies (listed in Table S6) at 4°C. The cells were washed again and fixed in Click-iT fixative for 15 min, washed once and then permeabilized in saponin-based permeabilization and wash reagent for 15 min. The Click-iT reaction cocktail was added to the cells for additional 30 min incubation. The cells were finally washed and analyzed by flow cytometry. All steps after the cell surface antibody staining were carried out at room temperature.

For *in vitro* cell cycle analysis of adult lung fibroblasts (ALFs), isolated ALFs (passage 1) were labeled with 20  $\mu$ M EdU. After 2h incubation, single cells were harvested by trypsinization and were processed as previously described according to the Click-iT EdU Flow Cytometry Assay. After the Click-iT reaction, the cells were counterstained for DNA content by Hoechst 33258 (1  $\mu$ g/mL) (Thermo Fischer) and analyzed by flow cytometry.

### CFSE cell proliferation assay of sorted CD8<sup>+</sup> T cell populations

To analyze the proliferative response of CD8<sup>+</sup> T cells upon TCR-dependent stimulation, splenic cell suspensions were prepared in 37°C pre-warmed PBS at a concentration of  $50 \times 10^6$  cells/mL and labeled with CFSE (Cayman Chemicals) at a concentration of 2.5  $\mu$ M for 10 min at 37°C in the dark. CFSE labeling was stopped by addition of 9 volumes of ice-cold T cell media (10% FBS, 1 mM non-essential amino acids, 1mM sodium pyruvate, 10 mM HEPES, 10 U/mL penicillin-10  $\mu$ g/mL streptomycin, 0.1 mM  $\beta$ -mercaptoethanol in RPMI 1640 with L-glutamine). The cells were washed and stained with surface antibodies (listed in Table S6) for cell sorting of CD8<sup>+</sup> T cell splenic populations according to the gating strategy shown in Figure 6A. Sorted cells were washed in T cell media and were seeded in straight bottom 96-well plates that were coated overnight at 4°C with 1  $\mu$ g/ml anti-CD3 and anti-CD28 antibodies. After 42h of incubation at 37°C with 5% CO<sub>2</sub>, dead cells were labeled with Propidium Iodide (0.08  $\mu$ g/mL) (Thermo Fischer) and CFSE dye dilution was analyzed by flow cytometry. The division index and proliferation index were calculated using the FlowJo version 10 proliferation tool. The division index depicts the average number of cell divisions completed by a cell of the original population (including undivided cells), while the proliferation index represents the number of cell divisions divided by the number of cells that completed at least one cell division.

### Competitive bone marrow reconstitution

Bone marrow (BM) cell suspensions from CD45.2 *Pole3*<sup>+/+</sup>, CD45.2 *Pole3*<sup>m3/m3</sup>, and CD45.1 wild-type mice (7-12 weeks of age) were prepared and an aliquot was stained with surface antibodies (listed in Table S6) for flow cytometric determination of HSCs. Two bone marrow cell suspensions of the desired donors, each containing 50 HSCs, were combined from the required sources before transplantation. The mixtures of CD45.1 and CD45.2 bone marrow cells were resuspended in 100  $\mu$ L PBS and transplanted into lethally irradiated (a total of 9.5 Gy delivered in two doses of 5 Gy and 4.5 Gy, separated by a 3h interval) CD45.1/2 heterozygote recipient mice (7-12 weeks of age) by tail vein injection. Peripheral blood was obtained from the recipient mice at 4, 8, 12 and 16 weeks after transplantation. Following red blood cell lysis, the contributions of CD45.2<sup>+</sup> donor derived cells to the T cell (CD3<sup>+</sup>), B cell (B220<sup>+</sup>) and myeloid (CD11b/Gr1<sup>+</sup>) lineages were assessed by flow cytometry (see antibodies in Table S6). At 16 weeks after transplantation, the mice were sacrificed and BM, thymus, spleen and lymph nodes were collected for flow cytometric analysis using the antibodies listed in Table S6.

### Analysis of TCR $\beta$ rearrangements

To determine the presence of TCR $\beta$  rearrangements, thymocyte suspensions were sorted into CD8<sup>+</sup> SP, CD4<sup>+</sup> SP and DP populations (using surface antibodies listed in Table S6), resuspended in 1x lysis buffer (10 mM Tris-HCl [pH 8.3], 50mM KCl, 0.01 mg/ml gelatin, 0.045% Nonidet P-40, 0.045% Tween20) including 0.1  $\mu$ g/ $\mu$ L Proteinase K and were incubated at 55°C for 1h to overnight and finally at 95°C for 10 min to inactivate the protease. TCR $\beta$  rearrangements were determined following a previously described method (Kawamoto et al., 2000). In brief, cell lysates were directly used as templates for PCR amplification using the following primers: D $\beta$ 2, 5'-GCACCTGTGGGAAGAACT-3'; J $\beta$ 2.6, 5'-TGAGAGCTGTCTCCTACTATCGATT3'. The PCR products were loaded on a 1.2% agarose gel and after electrophoresis were stained with GelRed for documentation.

### Image processing

Uneven light on image background and shadows were removed in Photoshop CC for photos of mouse embryos. For mouse skeletal images (Alcian Blue- Alizarin Red staining), focused z stack imaging consisting of multiple segmented tiles was performed in Photoshop CC to capture the embryo in its entirety.

### QUANTIFICATION AND STATISTICAL ANALYSIS

Graphs were generated and analyzed using the GraphPad Prism software. The data are shown as mean  $\pm$  s.e.m. Statistical significance was determined by unpaired two tailed t tests. *P* values of pairwise comparisons and number of animals (*n*) are depicted in each graph. Statistical details of experiments can be found in the figure legends.



**Cell Reports, Volume 31**

## **Supplemental Information**

### **Lymphocyte-Specific Function of the DNA Polymerase Epsilon Subunit Pole3 Revealed by Neomorphic Alleles**

**Iliana Siamishi, Norimasa Iwanami, Thomas Clapes, Eirini Trompouki, Connor P. O'Meara, and Thomas Boehm**



**Figure S1. Characterization of *Pole3* alleles, Related to Figures 1, 2.**

(A) Schematic representation of the mouse *Pole3* locus and the targeting replacement vector. The deletion cassette containing  $\beta$ -galactosidase and neomycin coding sequences replaces a genomic sequence of 1,056 bp spanning the entire encoding sequence of *Pole3*.

(B) Schematic representation of the predicted domains of mouse Pole3 and Pole4 proteins.

(C) Alignment of vertebrate POLE3 protein sequences using the EMBL-EBI Clustal Omega sequence alignment tool. Fully conserved residues are indicated by asterisk, residues with highly similar chemical properties are indicated by a colon, and those with related properties are denoted with a period. Genbank accession numbers: Human, NP\_001265184; mouse, NP\_067473; dog, XP\_855374; cat, XP\_003995820; chicken, NP\_001020525, zebrafish, NP\_957095.

(D) Relationship of the predicted secondary structures ( $\alpha$ -helices) of mouse Pole3 protein (top) to the exon/intron structure of the *Pole3* gene (bottom) with exons represented as squared boxes and introns as connecting lines. The color-coding indicates the contribution of exons to each structural motif of the Pole3 protein; numbers represent amino acid residues.

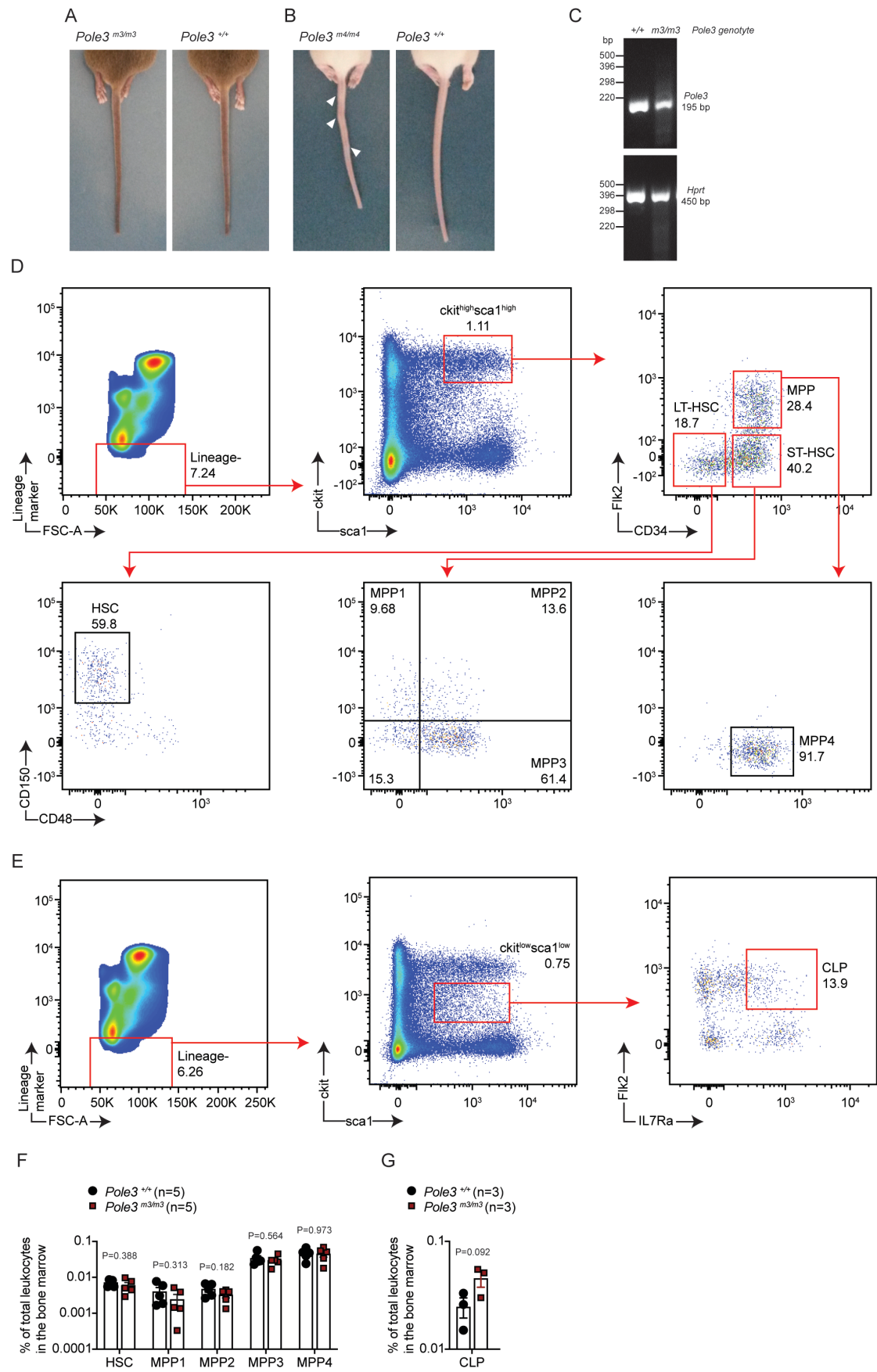


**Figure S2. Abnormal tail structure of *Pole3*<sup>m4/m4</sup> mice, Related to Figure 2.**

(A, B) Tails of adult *Pole3*<sup>m3/m3</sup> (A) and *Pole3*<sup>m4/m4</sup> (B) mice. Tail kinks in *Pole3*<sup>m4/m4</sup> mice are indicated with white arrowheads.

(C) RT-PCR analysis of *Pole3* (upper panel) and *Hprt* (lower panel) expression using RNA extracted from thymi of wild-type and *Pole3*<sup>m3/m3</sup> mice.

(D) Gating strategy for phenotypic analysis of the hematopoietic progenitor populations HSC, MPP1, MPP2, MPP3 and MPP4.

(E) Gating strategy for phenotypic analysis of the CLP population.

(F, G) Frequency of hematopoietic progenitor populations (F) and the CLP population (G) in the bone marrow in adult mice of the indicated genotypes. Bar graphs indicate means $\pm$ SEM. Significance levels as determined by t-test are indicated; each data point represents one mouse. Abbreviations, LT long-term; ST short term; HSC hematopoietic stem cell; MPP multipotent progenitor, CLP common lymphoid progenitor.



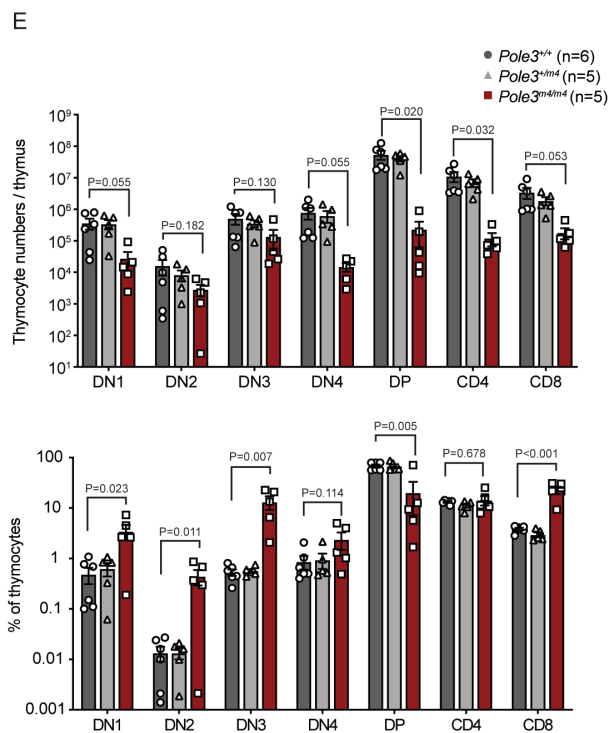
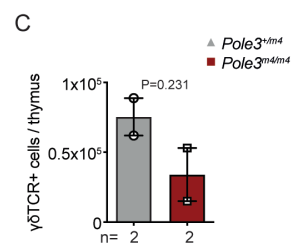
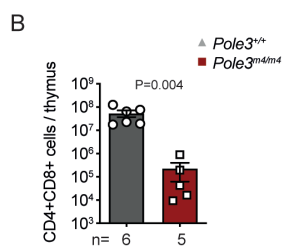
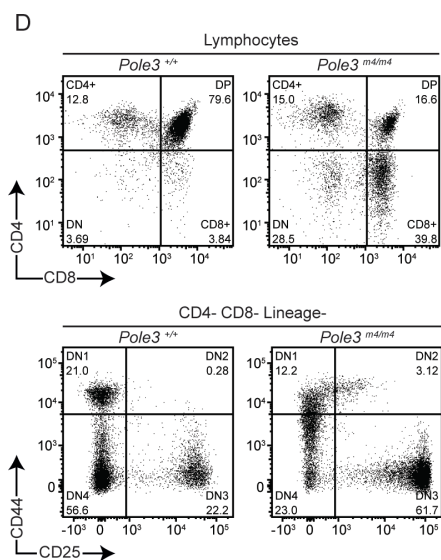
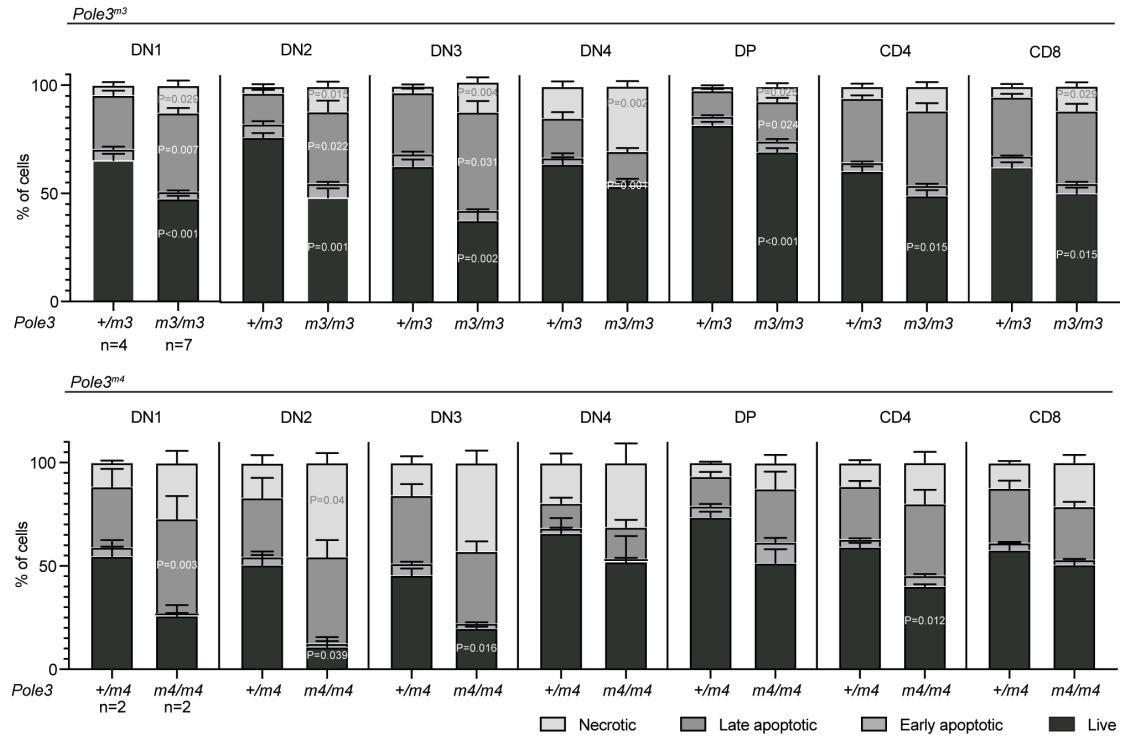


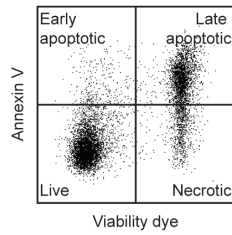
**Figure S3. Characterization of T cell development in adult mice carrying the *Pole3*<sup>m4</sup> allele, Related to Figure 3.**

- (A) Representative images of thymi and spleens taken at 5 weeks of age.
- (B) Total numbers of CD4<sup>+</sup>CD8<sup>+</sup> double-positive thymocytes.
- (C) Total cell numbers of  $\gamma\delta$  TCR<sup>+</sup> T cells in the thymus.
- (D) Flow cytometric profiles of adult thymocytes.
- (E) Thymocyte populations in adult mice of the indicated genotypes; absolute numbers are shown at the top, proportions are indicated at the bottom. Bar graphs indicate means $\pm$ SEM. Significance levels as determined by t-test are indicated; each data point represents one mouse.

B



A



C

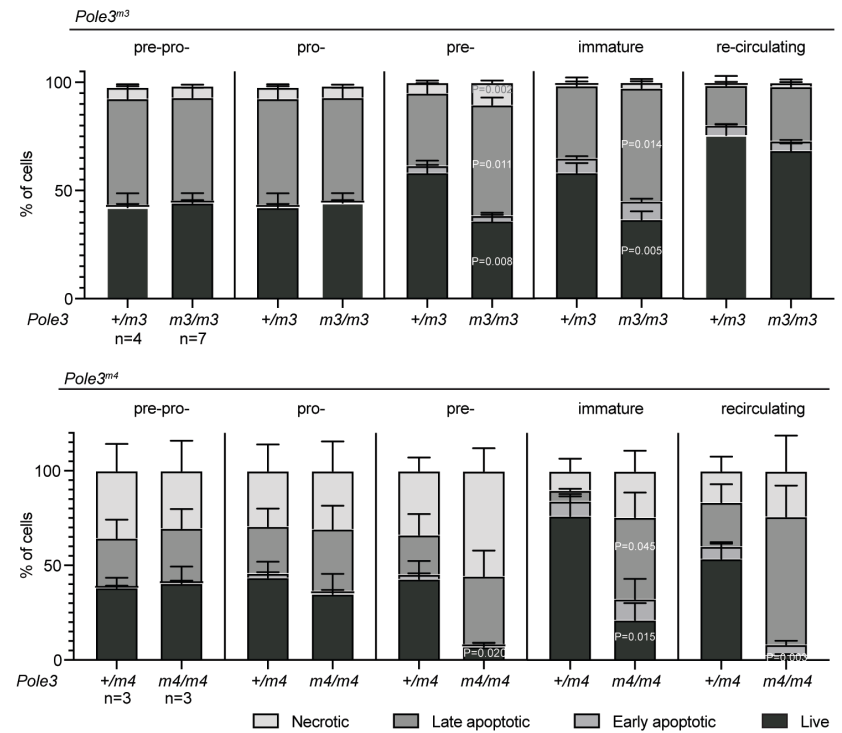


**Figure S4. Apoptosis in *Pole3* mutant lymphocytes, Related to Figures 3 and 4.**

(A) Gating strategy for the detection of apoptotic cells in differentiating lymphocyte populations.

(B, C) Frequency of live, early apoptotic, late apoptotic and necrotic cells in thymocyte populations in (B) in *Pole3<sup>m3</sup>* (upper panel) and *Pole3<sup>m4</sup>* (lower panel) adult mice and in differentiating B cell populations (C) in the bone marrow of *Pole3<sup>m3</sup>* (upper panel) and *Pole3<sup>m4</sup>* (lower panel) adult mice. Bar graphs indicate means $\pm$ SEM. Significance levels as determined by t-test are indicated where  $P < 0.05$ .

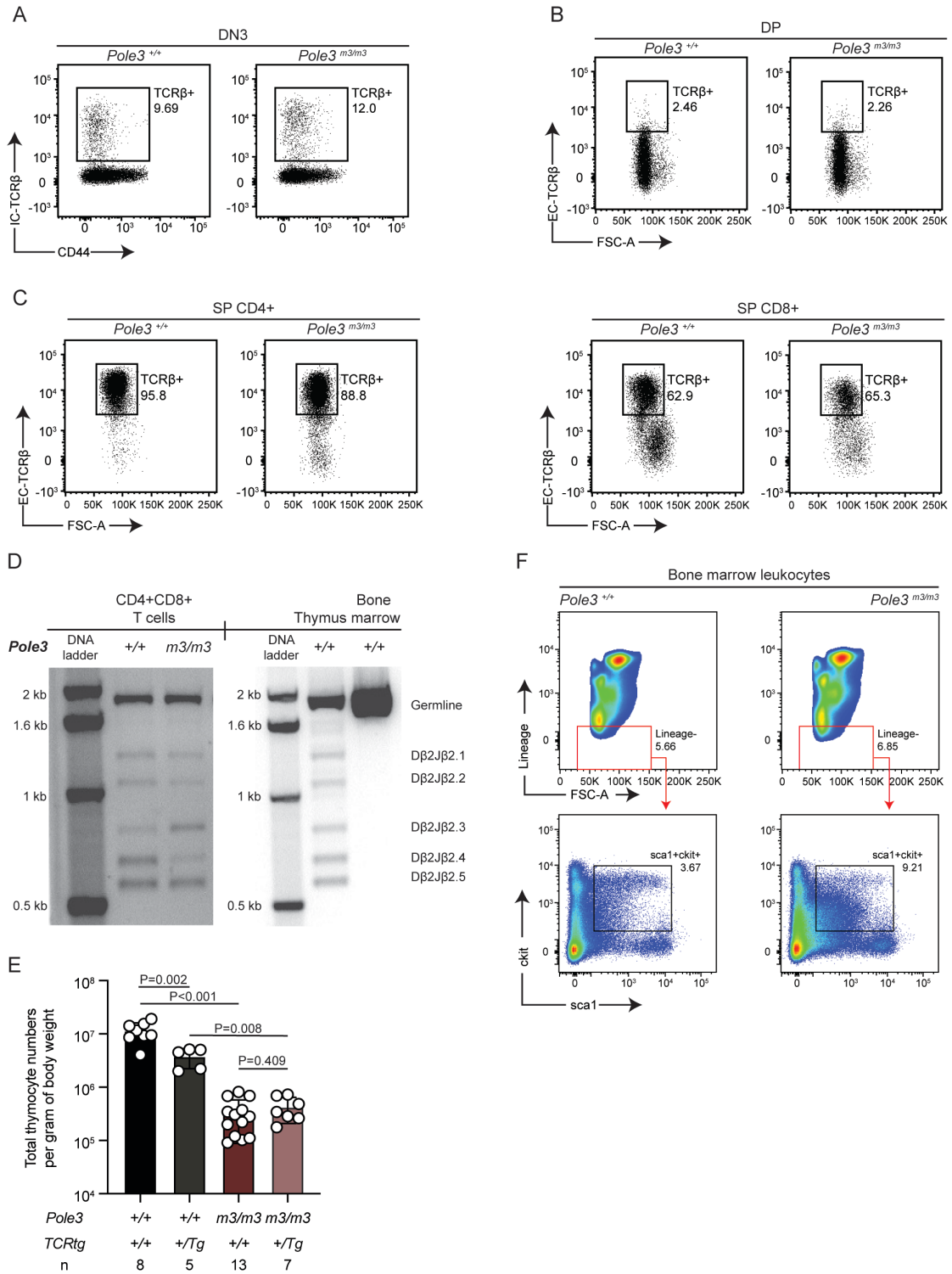




**Figure S5. Characterization of the TCR $\beta$  status in adult *Pole3*<sup>m3/m3</sup> mice, Related to Figure 6.**

(A) Intracellular TCR $\beta$  protein levels of DN3 thymocytes.

(B) Surface levels of TCR $\beta$  of DP thymocytes.

(C) Surface levels of TCR $\beta$  of single positive CD4<sup>+</sup> CD8<sup>+</sup> thymocytes. In (A-C), numbers indicate the percentages of cells in the indicated gates.

Abbreviations, IC, intracellular; EC, extracellular.

(D) D-J rearrangements of the *Tcrb2* gene in purified CD4<sup>+</sup>CD8<sup>+</sup> double-positive thymocytes (left panel) as examined by PCR. Whole thymocytes and total bone marrow cells of a wild-type mouse were used as positive and negative controls, respectively (right panel). (E) Total thymocyte numbers per gram of body weight in adult *Pole3*<sup>m3/m3</sup> mutant mice in the presence or absence of an  $\alpha\beta$ TCR transgene (Tg). Bar graphs indicate means $\pm$ SEM. Significance levels as determined by t-test are indicated; each data point represents one mouse.

(F) Representative flow cytometry plots indicating the increased expression levels of Sca1<sup>+</sup> on cells within the Lin<sup>-</sup>c-kit<sup>+</sup> cell population of the bone marrow of *Pole3*<sup>m3/m3</sup> mice. Numbers indicate percentages of cells in each gate.

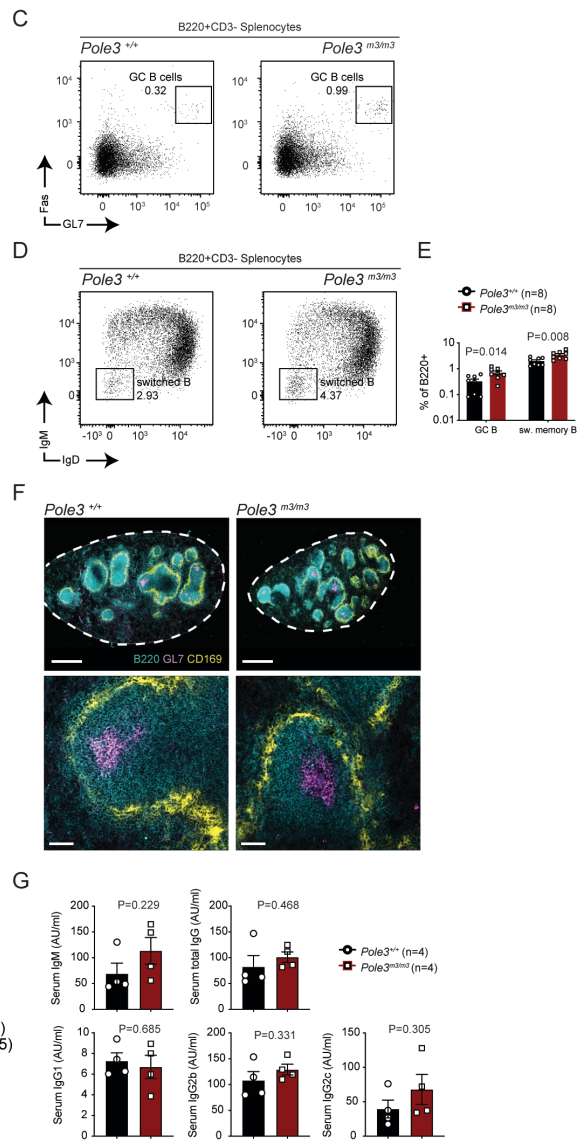
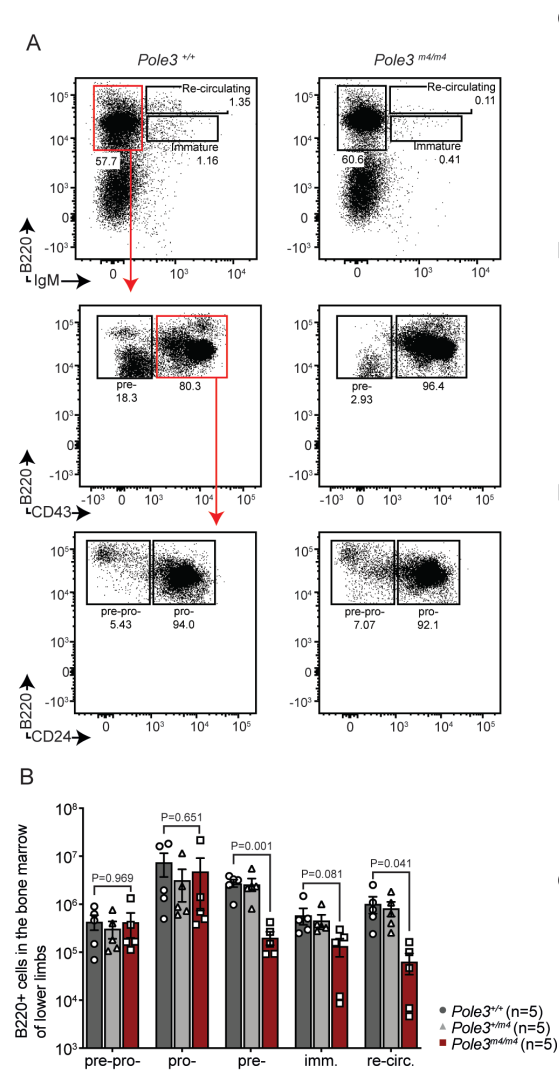
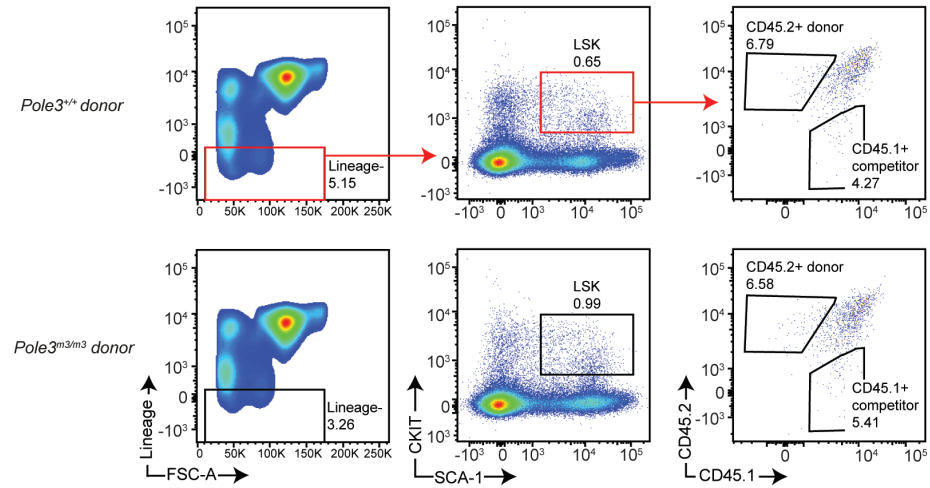


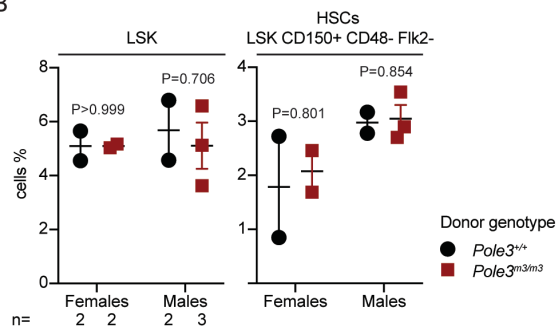
**Figure S6. Characterization of the adult B cell compartment in *Pole3<sup>m3/m3</sup>* and *Pole3<sup>m4/m4</sup>* mice, Related to Figure 4.**

- (A) Gating strategy applied for flow cytometric analysis of developmental B cell stages in the bone marrow of *Pole3<sup>m4</sup>* mice on the FVB genetic background. Numbers indicate percentage of cells in the respective gates.
- (B) Total numbers of B220<sup>+</sup> cells in each B cell stage of bone marrow taken from the lower limbs (combined cells of femur, tibia and pelvis). Abbreviations, imm. immature, re-circ. re-circulating.
- (C, D) Gating strategy for flow cytometric analysis of germinal center B cells (C) and switched memory B cells (D) in the spleen of *Pole3<sup>m3/m3</sup>* mice. Numbers indicate percentages of cells in each gate.
- (E) Proportion of germinal center B cells and switched memory B cells within the B220<sup>+</sup> cell compartment of the spleen. Abbreviations, GC germinal center, sw. switched.
- (F) Immunofluorescence staining of spleen sections from *Pole3<sup>m3</sup>* mice. Distribution of germinal centers (GL7<sup>+</sup>, violet) within B cell follicles (B220<sup>+</sup>, cyan). CD169<sup>+</sup> macrophages (yellow) mark the boundaries of the B cell follicles. Scale bar (upper panel) 100  $\mu$ m, (lower panel) 20  $\mu$ m.
- (G) Serum concentrations of IgM (upper left), total IgG (upper, right) and IgG subclasses IgG1 (bottom, left), IgG2b (bottom, middle) and IgG2c (bottom, right) as arbitrary units (AU) per mL serum. Bar graphs indicate means $\pm$ SEM. Significance levels as determined by t-test are indicated; each data point represents one mouse.

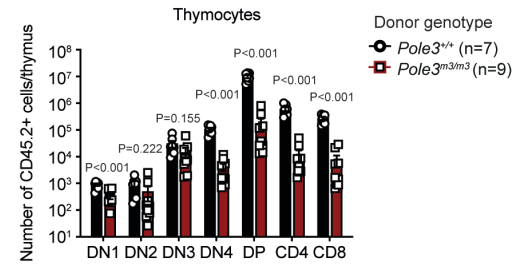
A



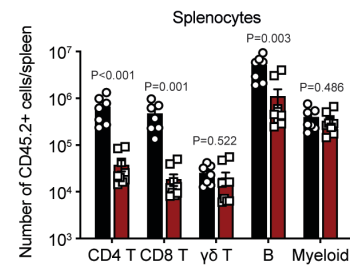
B



C



D



E



F

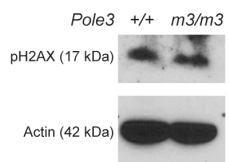


**Figure S7. Potency of hematopoietic cells of *Pole3*<sup>m3/m3</sup> mice, Related to Figure 5.**

(A) Presence of *Pole3*<sup>m3/m3</sup> mutant hematopoietic progenitors in the bone marrow of recipient mice, 16 hours after transplantation. The gating strategy identifying the LSK populations (Lin<sup>-</sup>;Sca1<sup>high</sup>;c-kit<sup>high</sup>) in CD45.2-expressing mutant and CD45.1-expressing wild-type competitor cells. Numbers indicate percentages of cells in the respective gates.

(B) Frequencies of wild-type and mutant CD45.2<sup>+</sup> donor cells within the LSK and HSC (LSK<sup>+</sup>CD150<sup>+</sup>CD48<sup>-</sup>Flk2<sup>-</sup>) fractions in female and male recipient mice, as determined 16 hours after transplantation. Bar graphs indicate means±SEM. Significance levels as determined by t-test are indicated; each data point represents one mouse.

(C-E) Total numbers of CD45.2<sup>+</sup> donor cells of the indicated genotypes in the thymus (C), spleen (D), and bone marrow (E) of recipient cells. Bar graphs indicate means±SEM. Significance levels as determined by t-test are indicated; each data point represents one mouse.

(F) Similar levels of phosphorylated (Ser139) H2AX histone in the thymus of *Pole3*<sup>m3/m3</sup> and control mice as shown by western blot.



**Table S1.** Genotype distribution at 3 weeks of age, related to Figure 2.

	+/+	+/ <i>m</i>	<i>m/m</i>
<i>Pole3</i> <sup><i>m1</i></sup>	13	23	17
<i>Pole3</i> <sup><i>m2</i></sup>	23	37	23
<i>Pole3</i> <sup><i>m3</i></sup>	120	259	107
<i>Pole3</i> <sup><i>m4</i></sup>	135	252	16

Genotype distribution of *Pole3* allelic variants at 3 weeks of age. The *Pole3*<sup>*m4/m4*</sup> is significantly underrepresented at this age; all other distributions conform to the expected Mendelian ratios.

**Table S2.** Body weight at 4-6 weeks of age, related to Figure 2.

	+/+	+/ <i>m</i>	<i>m/m</i>
<i>Pole3</i> <sup><i>m1</i></sup>	23.475±0.78 n=4	n.d.	20.52±1.93 n=5
<i>Pole3</i> <sup><i>m2</i></sup>	20.65±1.46 n=8	n.d.	20.1±1.39 n=11
<i>Pole3</i> <sup><i>m3</i></sup>	18.75±0.58 n=8	20.96±2.36 n=2	17.33±0.92 n=9
<i>Pole3</i> <sup><i>m4</i></sup>	20.98±0.91 n=9	19.78±0.67 n=7	16.01±1.23 n=8 *

Summary of body weights at 4-6 weeks of age (means±SEM; number of animals in each group is indicated). The weight of the *Pole3*<sup>*m4/m4*</sup> mice is significantly reduced (P=0.00493; t-test).

**Table S3.** guide RNA sequences (sgRNA) and DNA repair template for CRISPR-Cas9 mutagenesis, related to STAR Methods.

sgRNAs	Target sequence (5'>3')*	Single-stranded DNA repair template
sgRNA #1: <i>Pole3</i> <sup><i>m1</i></sup> , <i>Pole3</i> <sup><i>m2</i></sup>	TACAGGCGGGAGCAGAA	
sgRNA #2: <i>Pole3</i> <sup><i>m1</i></sup> , <i>Pole3</i> <sup><i>m2</i></sup>	ACGACCAGAACGAAGAG G	
sgRNA #3: <i>Pole3</i> <sup><i>m3</i></sup> , <i>Pole3</i> <sup><i>m4</i></sup>	CGGGAGCAGAAAGGCAA G	CGGTTTGTCTAATTAAACCATAATAT CCTGCTTCCTTACAGCGTACAGGC AGGAACAGAAGGGCAAGAAGGAGG CTTCGGAGCAAAAAGAAGAAGGACA AAGACAAAAAGGA

**Table S4.** Genotyping primers, related to STAR Methods.

Target	Forward primer (5'>3') Reverse primer (5'>3')	Amplicon size (bp)	Sequencing Primer (5'>3')
<b>Mouse</b>			
<i>Pole3</i> knockout	GCAGCCTCTGTTCCACATACACTTCA CTTTAGTGCTTCTGTGACTTGGAACA	493	
<i>Pole3</i> wild-type allele	GTGTGTTTCATCTCCACTCTCCTCGC ACCTGCTCCAGAATGTGTGACAACT	255	
<i>Pole3</i> <sup>m1</sup> , <i>Pole3</i> <sup>m2</sup> alleles	TGCTCATCAGTATCAGTGCC CGGTTTCTGTAACTCAGATGC	517 (wt) 385 (m1) 356 (m2)	
<i>Pole3</i> wildtype allele	TGCTCATCAGTATCAGTGCC TTCTGGTCGTCTCGTCCAG	305	
<i>Pole3</i> <sup>m3</sup> , <i>Pole3</i> <sup>m4</sup> alleles	CACCTGTGCCTCGGTTTGTG CATGTCTCAGGATCTCAGGG	277 (wt) 278 (m3) 279 (m4)	CATGTCTCAGGATCTCA GGG
<i>TCRtg</i>	CTGAGGCTGATCCATTACTC TAACACGAGGAGCCGAGTGCCT	216	

**Table S5.** RT-PCR Primers, related to STAR Methods.

Target	Forward primer (5'>3') Reverse primer (5'>3')	Amplicon size (bp)
<i>Pole3</i>	GAAGCTCTAGAAGCGTACAGG CCTACTCTCTCCATTCACTTG	195
<i>Hprt</i>	GATTATGGACAGGACTGAAAG CAAGGGCATATCCAACAACAACT	450

**Table S6.** Fluorescently labeled antibodies, related to STAR Methods.

Antigen/Staining Reagent	Clone	Conjugate	Source	Identifier
<b>Thymocyte stage analysis, related to Figures 1C, 3B-3F, and Figure S3</b>				
CD4	GK1.5	APC Cy7	Biolegend	100414
CD8a	53-6.7	PE	eBioscience	12-0081-85
CD44	IM7	APC	eBioscience	17-0441-81
CD25	PC61	PE Cy7	BD Biosciences	552880
B220 (CD45R)	RA3-6B2	FITC	Biolegend	103206
TCR $\gamma\delta$	eBioGL3	FITC	eBioscience	11-5711-82
NK1.1	PK136	FITC	Biolegend	108706
CD11c	HL3	FITC	BD Biosciences	557400
CD11b (Mac1)	M1/70	FITC	BD Biosciences	557396
<b>Annexin V detection in thymocytes, related to Figure S4A-S4B</b>				
CD4	GK1.5	PE Dazzle	Biolegend	100455
CD8a	53-6.7	BV421	Biolegend	100738
CD44	IM7	APC	eBioscience	17-0441-81
CD25	PC61	PE Cy7	BD Biosciences	552880
TCR $\gamma\delta$	GL3	PerCP Cy5.5	Biolegend	118118
B220 (CD45R)	RA3-6B2	PE	Biolegend	103208
NK1.1	PK136	PE	eBioscience	12-5941-83
CD11c	N418	PE	eBioscience	12-0114-82
CD11b (Mac1)	M1/70	PE	BD Biosciences	553311
<b>Thymocyte stages TCR-<math>\beta</math>, related to Figure S5A-S5C</b>				
CD4	GK1.5	APC Cy7	Biolegend	100414
CD8a	53-6.7	BV421	Biolegend	100738
CD44	IM7	APC	eBioscience	17-0441-81
CD25	PC61	PE Cy7	BD Biosciences	552880
B220 (CD45R)	RA3-6B2	FITC	Biolegend	103206
NK1.1	PK136	FITC	Biolegend	108706
CD11c	HL3	FITC	BD Biosciences	557400
CD11b (Mac1)	M1/70	FITC	BD Biosciences	557396
TCR $\gamma\delta$	GL3	PerCP Cy5.5	Biolegend	118118
TCR- $\beta$	H57-597	PE	eBioscience	12-5961-83
<b>Thymocyte stages CXCR4, related to Figure 3G-3H</b>				
CD4	GK1.5	APC Cy7	Biolegend	100414
CD8a	53-6.7	BV421	Biolegend	100738
CD44	IM7	APC	eBioscience	17-0441-81
CD25	PC61	PE Cy7	BD Biosciences	552880
B220 (CD45R)	RA3-6B2	FITC	Biolegend	103206
NK1.1	PK136	FITC	Biolegend	108706
CD11c	HL3	FITC	BD Biosciences	557400
CD11b (Mac1)	M1/70	FITC	BD Biosciences	557396
TCR $\gamma\delta$	GL3	PerCP Cy5.5	Biolegend	118118
CXCR4 (CD184)	L276F12	PE	Biolegend	146506
<b>Thymocyte stages SCA1, related to Figure 3I-3J</b>				
CD4	GK1.5	APC Cy7	Biolegend	100414
CD8a	53-6.7	BV421	Biolegend	100738
CD44	IM7	PE	BD Biosciences	553134
CD25	PC61	Alexa Fluor 647	Biolegend	102020
B220 (CD45R)	RA3-6B2	FITC	Biolegend	103206
NK1.1	PK136	FITC	Biolegend	108706
CD11c	HL3	FITC	BD Biosciences	557400
CD11b (Mac1)	M1/70	FITC	BD Biosciences	557396
TCR $\gamma\delta$	GL3	PerCP Cy5.5	Biolegend	118118
Sca1 (Ly-6A/E)	D7	PE Cy7	Biolegend	108113
<b>Thymocyte stages sort, related to Figure S5D</b>				
CD4	GK1.5	APC Cy7	Biolegend	100414
CD8a	53-6.7	BV421	Biolegend	100738
CD44	IM7	PE	BD Biosciences	553134
CD25	PC61	Alexa Fluor 647	Biolegend	102020
B220 (CD45R)	RA3-6B2	FITC	Biolegend	103206
TCR $\gamma\delta$	eBioGL3	FITC	eBioscience	11-5711-82
NK1.1	PK136	FITC	Biolegend	108706

CD11c	HL3	FITC	BD Biosciences	557400
CD11b (Mac1)	M1/70	FITC	BD Biosciences	557396
<b>B cell stage analysis, related to Figure 2H, Figure 4, and Figure S6A-S6B</b>				
IgM	II/41	FITC	BD Biosciences	553437
BP-1 (Ly51)	6C3	PE	Thermo Fischer	12-5891-83
CD43	S7	APC	BD Biosciences	560663
B220 (CD45R)	RA3-6B2	PE Cy7	eBioscience	25-0452-82
CD24	M1/69	eFluor® 450	eBioscience	48-0242-82
<b>Annexin V detection in B cells in the bone marrow, related to Figures S4A, and S4C</b>				
IgM	II/41	PE	eBioscience	12-5790-81
CD43	S7	APC	BD Biosciences	560663
B220 (CD45R)	RA3-6B2	PE Cy7	eBioscience	25-0452-82
CD24	M1/69	eF450	eBioscience	48-0242-82
CD3	145-2C11	PerCP Cy5.5	Biolegend	100328
<b>Germinal center B cells in the spleen, related to Figure S4C, and S4E</b>				
CD3	145-2C11	PE	Biolegend	100308
B220 (CD45R)	RA3-6B2	FITC	Biolegend	103206
Fas (CD95)	SA367H8	APC	Biolegend	152603
GL7	GL7	BV421	BD Biosciences	562967
<b>Switched memory B cells in the spleen, related to Figure S4D, and S4E</b>				
CD3	145-2C11	PE	Biolegend	100308
B220 (CD45R)	RA3-6B2	FITC	Biolegend	103206
IgM	II/41	eFluor® 450	eBioscience	48-5790-82
IgD	11-26c.2a	Alexa Fluor® 647	Biolegend	405707
<b>Germinal centers in spleen sections, related to Figure S4F</b>				
GL7	GL7	Alexa Fluor488	Biolegend	144612
B220 (CD45R)	RA3-6B2	Alexa Fluor® 647	BD Biosciences	557683
CD169 (Siglec-1)	3D6.112	BV421	Biolegend	142421
<b>Peripheral lymphocyte analysis, related to Figure 3C, and S3C</b>				
CD4	GK1.5	APC Cy7	Biolegend	100414
CD8a	53-6.7	BV421	Biolegend	100738
TCR γδ	GL3	PerCP Cy5.5	Biolegend	118118
B220 (CD45R)	RA3-6B2	FITC	Biolegend	103206
CD11c	HL3	FITC	BD Biosciences	557400
CD11b (Mac1)	M1/70	FITC	BD Biosciences	557396
CD3e	145-2C11	APC	Thermo Fischer	17-0031-82
α-GalCer Loaded CD1 tetramer		PE	ProlImmune	E001-2X
<b>EdU incorporation in Thymus, related to Figure 7C-7D</b>				
CD4	GK1.5	APC Cy7	Biolegend	100414
CD8a	53-6.7	BV421	Biolegend	100738
CD44	IM7	APC	eBioscience	17-0441-81
CD25	PC61	BV605	Biolegend	102035
<b>Peripheral lymphocyte analysis, related to Figure 2C-2G, and 6</b>				
CD8a	53-6.7	PE Cy7	eBioscience	25-0081-82
CD4	GK1.5	PE Dazzle	Biolegend	100455
TCRβ	H57-597	BV421	Biolegend	109229
CD62L	MEL-14	Alexa Fluor® 700	Biolegend	104426
CD44	IM7	APC	eBioscience	17-0441-81
CD19	eBio1D3	PE	eBioscience	12-0193-83
<b>HSC-MPP phenotyping, related to Figure S2D, and S2F</b>				
CD3e	145-2C11	FITC	Biolegend	100306
B220 (CD45R)	RA3-6B2	FITC	Biolegend	103206
CD11b (Mac1)	M1/70	FITC	BD Biosciences	557396
Gr1 (Ly-6G/Ly-6C)	RB6-8C5	FITC	Biolegend	108406
TER-119	TER-119	FITC	eBioscience	11-5921-81
Sca1 (Ly-6A/E)	D7	APC	eBioscience	17-5981-81
Ckit (CD117)	2B8	BV421	Biolegend	105827
Flk2 (CD135)	A2F10.1	PE	BD Biosciences	561068
CD34	RAM34	Alexa Fluor® 700	eBioscience	56-0341-82
CD150 (SLAMF)	TC15-12F12.2	BV605	Biolegend	115927
CD48	HM48-1	APC Cy7	Biolegend	103431
<b>CLP phenotyping, related to Figure S2E, and S2G</b>				
CD3e	145-2C11	FITC	Biolegend	100306

B220 (CD45R)	RA3-6B2	FITC	Biolegend	103206
CD11b (Mac1)	M1/70	FITC	BD Biosciences	557396
Gr1 (Ly-6G/Ly-6C)	RB6-8C5	FITC	Biolegend	108406
TER-119	TER-119	FITC	eBioscience	11-5921-81
Sca1 (Ly-6A/E)	D7	APC	eBioscience	17-5981-81
Ckit (CD117)	2B8	BV421	Biolegend	105827
IL-7Ra	A7R34	PE Dazzle	Biolegend	135031
Flk2 (CD135)	A2F10	PerCP efluor710	eBioscience	46-1351-80
<b>Peripheral blood reconstitution, related to Figure 5A-5E</b>				
CD45.1	A20	PE	eBioscience	12-0453-83
CD45.2	104	BV421	Biolegend	109831
CD11b (Mac1)	M1/70	FITC	BD Biosciences	557396
Gr1 (Ly-6G/Ly-6C)	RB6-8C5	FITC	Biolegend	108406
CD3e	145-2C11	APC	Thermo Fischer	17-0031-82
B220 (CD45R)	RA3-6B2	PE Cy7	eBioscience	25-0452-82
<b>HSC engraftment analysis, related to Figure S7A-S7B</b>				
CD3e	145-2C11	FITC	Biolegend	100306
B220 (CD45R)	RA3-6B2	FITC	Biolegend	103206
CD11b (Mac1)	M1/70	FITC	BD Biosciences	557396
Gr1 (Ly-6G/Ly-6C)	RB6-8C5	FITC	Biolegend	108406
Ter119	TER-119	FITC	eBioscience	11-5921-81
Sca1 (Ly-6A/E)	D7	PE Cy7	Biolegend	108113
CD48	HM48-1	PerCP efluor710	eBioscience	46-0481-82
CD150 (SLAMF6)	TC15-12F12.2	PE Dazzle	Biolegend	115935
Flk2 (CD135)	A2F10.1	PE	BD Biosciences	561068
CD45.2	104	Alexa Fluor 700	Biolegend	109822
CD45.1	A20	APC Cy7	Biolegend	110716
<b>Thymocyte engraftment analysis, related to Figure 5F, and S7C</b>				
CD4	GK1.5	PE Cy7	Biolegend	100422
CD8	53-6.7	BV421	Biolegend	100738
CD44	IM7	PE	BD Biosciences	553134
CD25	PC61	BV605	Biolegend	102035
TCR $\gamma\delta$	GL3	PerCP Cy5.5	Biolegend	118118
B220 (CD45R)	RA3-6B2	FITC	Biolegend	103206
NK1.1	PK136	FITC	Biolegend	108706
CD11c	HL3	FITC	BD Biosciences	557400
CD11b (Mac1)	M1/70	FITC	BD Biosciences	557396
CD45.2	104	Alexa Fluor 700	Biolegend	109822
CD45.1	A20	APC Cy7	Biolegend	110716
<b>Analysis of B cell engraftment in the bone marrow, related to Figure 5I, and S7E</b>				
IgM	II/41	FITC	BD Biosciences	553437
CD43	S7	PE	BD Biosciences	553271
B220 (CD45R)	RA3-6B2	PE Cy7	eBioscience	25-0452-82
CD24	M1/69	eF450	eBioscience	48-0242-82
CD45.2	104	Alexa Fluor 700	Biolegend	109822
CD45.1	A20	APC Cy7	Biolegend	110716
<b>Analysis of engraftment of peripheral leukocytes, related to Figure 5G-5H, and S7D</b>				
CD4	GK1.5	PE Cy7	Biolegend	100422
CD8	53-6.7	BV421	Biolegend	100738
B220 (CD45R)	RA3-6B2	FITC	Biolegend	103206
TCR $\gamma\delta$	GL3	PerCP Cy5.5	Biolegend	118118
CD11b (Mac1)	M1/70	PE	BD Biosciences	553311
Gr1 (Ly-6G/Ly-6C)	RB6-8C5	PE	Biolegend	108408
CD45.2	104	Alexa Fluor 700	Biolegend	109822
CD45.1	A20	APC Cy7	Biolegend	110716